J. Fluid Mech. (1993), *vol.* 249, *pp.* 557–596

The drag on an undulating surface induced by the flow of a turbulent boundary layer

By S. E. BELCHER, T. M. J. NEWLEY† AND J. C. R. HUNT

Department of Applied Mathematics and Theoretical Physics, University of Cambridge, Silver Street, Cambridge, CB3 9EW, UK

(Received 7 September 1991)

We investigate, using theoretical and computational techniques, the processes that lead to the drag force on a rigid surface that has two-dimensional undulations of length L and height H (with $H/L \ll 1$) caused by the flow of a turbulent boundary layer of thickness h. The recent asymptotic analyses of Sykes (1980) and Hunt, Leibovich & Richards (1988) of the linear changes induced in a turbulent boundary layer that flows over an undulating surface are extended in order to calculate the leading-order contribution to the drag. It is assumed that L is much less than the natural lengthscale $h_* = hU_0/u_*$ over which the boundary layer evolves (u_* is the unperturbed friction velocity and U_0 a mean velocity scale in the approach flow). At leading order, the perturbation to the drag force caused by the undulations arises from a pressure asymmetry at the surface that is produced by the thickening of the perturbed boundary layer in the lee of the undulation. This we term *non-separated sheltering* to distinguish it from the mechanism proposed by Jeffreys (1925). Order of magnitude estimates are derived for the other mechanisms that contribute to the drag; the next largest is shown to be smaller than the non-separated sheltering effect by $O(u_*/U_0)$. The theoretical value of the drag induced by the non-separated sheltering effect is in good agreement with both the values obtained by numerical integration of the nonlinear equations with a second-order-closure model and experiments. Although the analytical solution is developed using the mixing-length model for the Reynolds stresses, this model is used only in the inner region, where the perturbation shear stress has a significant effect on the mean flow. The analytical perturbation shear stresses are approximately equal to the results from a higher-order closure model, except where there is strong acceleration or deceleration. The asymptotic theory and the results obtained using the numerical model show that the perturbations to the Reynolds stresses in the outer region do not directly contribute a significant part of the drag. This explains why several previous analyses and computations that use the mixing-length model inappropriately throughout the flow lead to values of the drag force that are too large by up to 100%.

1. Introduction

Which physical process is dominant in inducing the drag on undulating topography below a turbulent boundary layer? This question remains largely unanswered. Furthermore, the magnitude of the resulting drag has no generally accepted value. Recent reviews of the drag induced by undulating surfaces have been written by Taylor, Mason & Bradley (1989) and Hunt *et al.* (1991). The change, induced by the

† Present address: c/o BP Exploration, Fairbanks, Alaska, USA.

undulation, in the drag force has important practical implications, particularly in meteorology. A key mechanism controlling the large-scale atmospheric motions is the transfer of momentum between the atmospheric boundary layer and the surface of the Earth. The large-scale numerical models that predict global climate typically have a spatial resolution on the order of 100 Km and, in order to model the momentum budget realistically, these climate models must account for the effects of the smaller-scale topographic features (subgridscale effects) that cannot be resolved explicitly. This is done by defining, for each grid element of the model, a roughness length that reflects the momentum exchange caused by the subgridscale effects. Recently, submesoscale numerical models have been used to estimate these roughness lengths for particular terrain and atmospheric conditions (Mason 1986*a*). Estimates of the dependence of the momentum exchange on the shape and lengthscale of the terrain and atmospheric conditions cannot be made systematically without a better understanding of the mechanisms that induce the drag. We focus on two-dimensional undulations and present a systematic investigation of the inter-relationship between the key drag mechanisms which should help the development of general formulae and guide future numerical and experimental studies.

The drag force on the surface is a result of the effect of the turbulent Reynolds stresses on the mean flow, since there would be no net force in a purely inviscid flow. Hence, in order to understand the physical mechanisms that enhance the force, the effect of the Reynolds stresses on the mean motions must be considered carefully. In §5 we investigate the structure of the perturbations to the turbulence using theoretical scaling arguments and the results of numerical modelling. In the numerical study, which is described in §4, the nonlinear Reynolds-averaged momentum equations are integrated with two models for the Reynolds stresses: the mixing-length model and the second-order-closure model of Launder, Reece & Rodi (1975). (Details of the numerical techniques and results of the velocity field have been reported by Newley 1986 and Hunt, Newley & Weng 1990). In the flows of interest, the lengthscale L of the perturbation is short compared to the relaxation lengthscale of the boundary layer, $h_* = hU_0/u_*$, where h is the boundary layer depth, U_0 is a characteristic value of the upwind mean flow (defined in §2 to be the value at the top of the middle layer) and u_* is the approach flow friction velocity. In this limit, the perturbations to the turbulence are shown here to be governed by different dynamics in different regions of the flow. We thereby derive important constraints on the type of turbulence closure that can model the changes to the Reynolds stresses in such a boundary layer. These conclusions are applicable to turbulent boundary layers that are perturbed in a variety of ways; they are not specific to the flow over an undulation (see §5.4).

The drag force resulting from each of the physical mechanisms is investigated by extending the asymptotic theories developed by Sykes (1980) and Hunt, Leibovich & Richards (1988, referred to herein as HLR), which describe the linear changes to a turbulent boundary layer flowing over a hill of height H, with $H/L \ll 1$. The theory is based on the technique developed for perturbed laminar boundary layers of dividing the flow into layers where different dynamical processes dominate. In the laminar boundary layer flow over an obstacle, the 'triple deck' method pioneered and subsequently reviewed by Stewartson (1974), can be used to describe the flow (Smith *et al.* 1981). In the case of turbulent boundary-layer flows, different forms of the governing equations are necessary in the different regions since the dominant behaviour of the Reynolds stresses changes through the flow. In §2, general arguments are used to derive the asymptotic structure of the perturbed turbulent boundary layer based on the assumptions that $H/L \ll 1$, $L \ll h_*$ and $u_*/U_0 \ll 1$. The analytical model

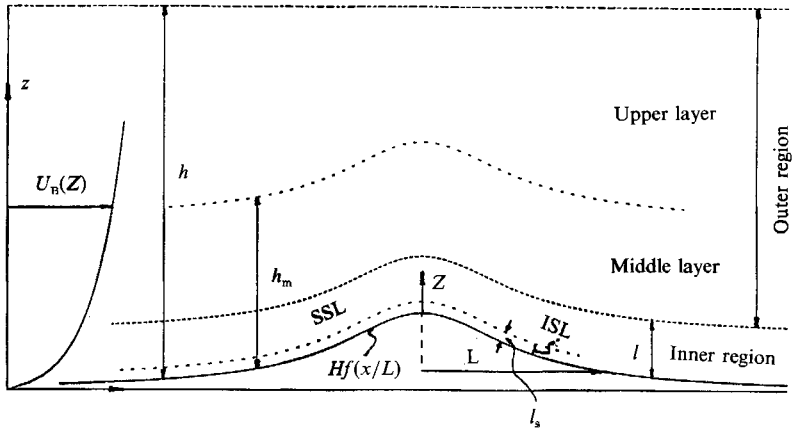

FIGURE 1. Flow geometry and asymptotic structure.

uses the simplest turbulence model that is consistent with the results of §5; namely, mixing length in the inner region and rapid distortion theory in the outer region. After evaluating higher-order terms in the theory for the velocity field, an explicit formula is derived for the drag.

1.1. *Classification of the drag mechanisms*

The change to the drag force on the surface may be written as

$$\Delta F = \rho U_0^2 L \lambda, \tag{1.1}$$

where ρ is the density of the boundary-layer fluid, L is the length from the hill summit to a point at half this height and λ is the dimensionless drag coefficient, which characterizes the effect of the undulation on the drag. Previous theoretical and numerical investigations of turbulent boundary-layer flow over undulating terrain have suggested various mechanisms to account for the drag force. We propose that these mechanisms may be classified, and their effect on the drag estimated, as follows (refer to figures 1 and 2*a–d*):

Non-separated sheltering (NSS) (figure 2a)

The actions of the Reynolds stresses close to the surface, in the inner region of depth l, cause a thickening of the boundary layer on the leeside of the hill and, thence, to separation of the mean flow when the slope is large enough. The thickness of the inner region is therefore asymmetric and so the largely inviscid outer-region flow is asymmetrically displaced downwind of the hill crest which leads to an out-of-phase component to the pressure perturbation. The contribution to λ from the non-separated sheltering effect may then be estimated (see §3 below) as

$$\lambda_{\mathrm{NSS}} = O\left(\frac{H}{L}\frac{l}{L}\mathrm{Asym}\left[\frac{\Delta u^{(\mathrm{I})}}{U_0}\right]\right) = O\left(\frac{H}{L}\frac{l}{L}\frac{H}{L}\epsilon\right), \tag{1.2}$$

where $\epsilon = u_*/U_0$ is the non-dimensional friction velocity and $\mathrm{Asym}[\Delta u^{(\mathrm{I})}]$ denotes the asymmetric part of the streamwise velocity perturbation in the inner region. This mechanism is related to Jeffreys' (1925) sheltering hypothesis, which was developed for separated flows over moving waves of large slope to account for their growth.

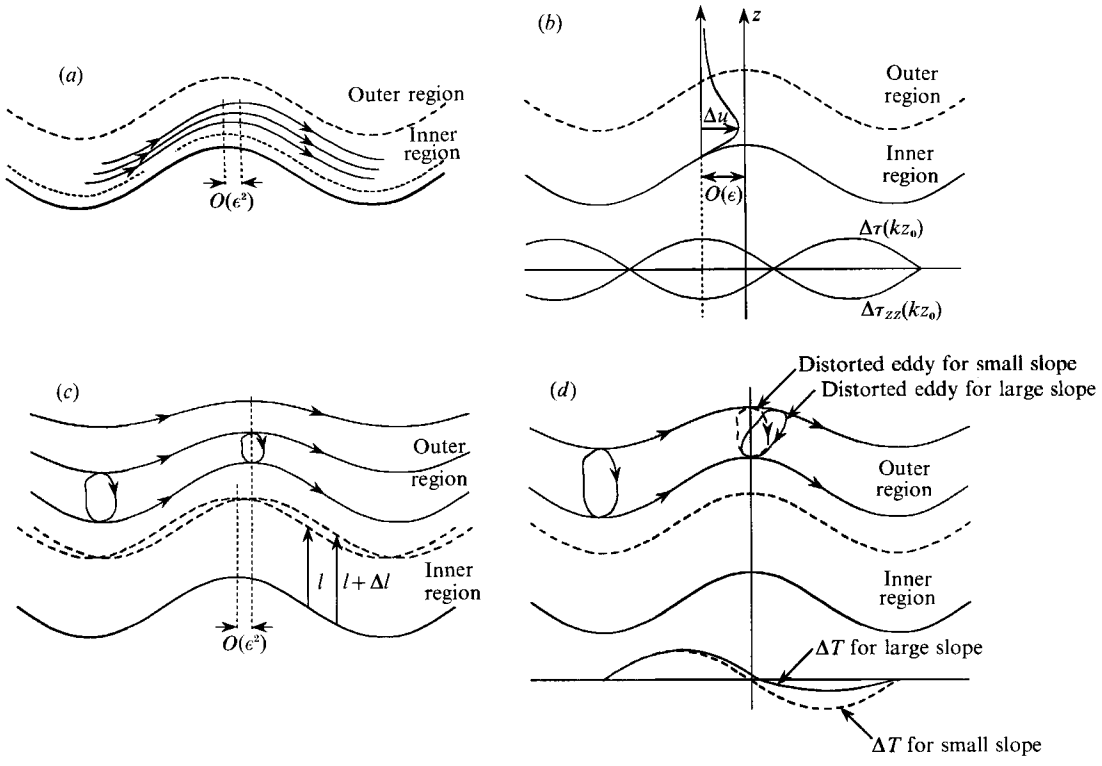

FIGURE 2. (*a*) *Non-separated sheltering.* The perturbed boundary layer thickens on the leeside of the crest due to the action of the shear stress in the inner region; thereby leading to a pressure asymmetry in the outer region. (*b*) *Inner-region Reynolds-stress effects.* Towards the surface the turbulence tends to a local equilibrium structure, so that the Reynolds-stress perturbations are determined by the local velocity gradient. The asymmetry in the inner region leads to perturbations to the Reynolds stresses that are out of phase and hence the Reynolds normal stresses are out of phase at the surface. This changes the drag. (*c*) ***Outer-region Reynolds-stress effects.*** The 'non-separated' sheltering in the inner region leads to a change, Δl, in the displacement of the largely inviscid outer-region flow. Consequently, the (rapid) distortion of the Reynolds stresses in the outer region is displaced downwind of the crest, thereby contributing to the drag. (*d*) *Finite-amplitude-distortion effects.* For larger slopes the distortion (and travel time or drift, ΔT) of the eddies is different along adjacent streamlines and so the distortion is not exactly in phase with the mean streamlines.

Inner-region Reynolds-stress effects (IRS) (figure 2b)

Within the inner region, the turbulence tends to a local equilibrium so that it adjusts to the local velocity gradient. The asymmetry of the mean flow, and the mean velocity gradients, in the perturbed boundary layer lead to asymmetrical perturbations in both the normal and shear Reynolds stresses. These additional asymmetries lead to changes in the pressure and thence to the force on the boundary (Townsend 1972, 1980). The perturbations to the Reynolds stresses in the inner region, $\Delta\tau^{(\mathrm{I})}$, scale on u_*^2, so that λ_{IRS}, the drag coefficient associated with this effect, may be estimated as

$$\lambda_{\mathrm{IRS}} = O\left(\frac{H}{L}\frac{u_*^2}{U_0^2}\mathrm{Asym}\left[\frac{\Delta\tau}{u_*^2}\right]\right) = O\left(\frac{H}{L}\frac{u_*^2}{U_0^2}\frac{H}{L}\epsilon\right), \tag{1.3}$$

see §6.1.

Outer-region Reynolds-stress effects (ORS) (figure 2c)

The distortion to the turbulent eddies in the outer region is determined by the history of the strain by the mean flow and may be calculated using rapid distortion theory (§5.3.2). The mean flow in the outer region is displaced slightly downwind of the hill crest by the non-separated sheltering and so the distortion of the turbulence in the outer region is slightly out of phase with the topography. This effect also leads to a drag, whose coefficient may be estimated (§6.2) as

$$\lambda_{\mathrm{ORS}} = O\left(\frac{u_*^2}{U_0^2}\lambda_{\mathrm{NSS}}\right) = O\left(\frac{H^2}{L^2}\frac{u_*^2}{U_0^2}\frac{l}{L}\epsilon\right). \tag{1.4a}$$

This mechanism was first suggested by the work of Sykes (1980). In a related calculation of the growth of water waves, Jacobs (1987) has attributed the leading-order asymmetric changes to the boundary layer to the effects of the Reynolds stresses in the outer region; this is not in agreement with the present analysis, as is discussed in §5.3.1.

The outer-region Reynolds stresses are also affected by the curvature of the mean streamlines. The linearized effects of the curvature lead, through the rapid distortion mechanism, to significant changes in the turbulence (Zeman & Jensen 1987) and thence to a linear pressure perturbation that is in anti-phase with the undulation. As discussed in §6.3, this pressure enhances the non-separated sheltering and thereby induces a contribution to the drag of magnitude

$$\lambda_{\mathrm{SC}} = O\left(\frac{H^2}{L^2}\frac{u_*^2}{U_0^2}\frac{l}{L}\epsilon\right). \tag{1.4b}$$

Effects of finite-amplitude distortion (FAD) (figure 2d)

At higher values of H/L, it may also be significant to consider the asymmetry in the Reynolds stresses produced by a finite-amplitude distortion to the flow. There is a nonlinear drift, of $O(H^2/L^2)$, of fluid elements (Hunt 1973) and hence the rapid distortion of the turbulence in the outer region is out of phase with the surface (Townsend 1980). This leads to a contribution to the drag coefficient, which may be estimated as

$$\lambda_{\mathrm{FAD}} = O\left(\frac{H}{L}\frac{H^2}{L^2}\frac{u_*^2}{U_0^2}\right) = O\left(\frac{H}{L}\lambda_{\mathrm{NSS}}\right). \tag{1.5}$$

The remainder of the paper is organized as follows. The analytical model is formulated, and the asymptotic structure developed, in §2. In §2.3 the asymmetric pressure perturbation is shown to play a central role in determining the drag. The analytical model is extended in §3 to calculate an explicit formula for the asymmetric pressure associated with the non-separated sheltering. In §4 the numerical model is described. The effects of the undulation on the turbulence dynamics are investigated in §5 using the results of the numerical simulations augmented with theoretical scalings. Thence, in §6, estimates are derived for the contributions to the asymmetric pressure from the other effects described above. An explicit formula for the drag is calculated in §7, which, in §8, is compared with the present numerical results and other experimental and computational studies.

2. The analytical model

2.1. *Definition and equations*

Consider a fully developed turbulent boundary layer over a surface, of roughness length z_0, that has a small two-dimensional undulation, see figure 1. The upwind velocity profile is $U_B(z)$, which is assumed steady on a timescale long compared with the time for an eddy to be advected over the hill. The unperturbed velocity profile is assumed to be logarithmic near the surface, in the inner region (defined below), so that the shear stress in the approach flow, τ_B, is constant and equal to ρu_*^2 in the inner region (u_* is the upwind friction velocity). Above, in the outer region, U_B may take a more general form. The surface is described by $z_s^* = Hf(x^*/L)$, where H is the height, L is the half-length (the length between the summit and a point at half the hill height), a lengthscale for the hill (or the perturbation in general). The undulation is assumed small so that one of the small parameters of the problem is $H/L \ll 1$.

The leading-order pressure perturbation develops in the middle layer (defined in §2.2.2) at a height of order h_m above the surface, so a suitable value on which to make the mean velocities non-dimensional is the value of the upwind velocity at h_m, $U_0 = U_B(h_m)$, and then the pressure perturbation is naturally made non-dimensional on ρU_0^2. All components of the Reynolds stresses are made non-dimensional on ρu_*^2, where u_* is the upwind friction velocity. Finally, the coordinates (x^*, z^*) are made non-dimensional on L.

The flow variables are expressed as the unperturbed values for flow over flat ground plus a small perturbation (e.g. Δu) caused by the presence of the topography. Furthermore, the leading-order pressure induced by the hill, which drives the perturbed flow, scales on H/L, so that the perturbed quantities may be expanded as power series in the slope (see HLR). The expansions hence proceed as follows:

$$u^* = U_B + \Delta u, \qquad \text{where } \Delta u = U_0\left(\frac{H}{L}u^{[1]} + \frac{H^2}{L^2}u^{[2]} + \ldots\right), \tag{2.1a}$$

$$w^* = \Delta w, \qquad \text{where } \Delta w = U_0\left(\frac{H}{L}w^{[1]} + \frac{H^2}{L^2}w^{[2]} + \ldots\right), \tag{2.1b}$$

$$\tau_{\alpha\alpha}^* = T_{\alpha\alpha} + \Delta\tau_{\alpha\alpha}, \qquad \text{where } {}^{\Delta\tau}_{\alpha\alpha} = \rho u_*^2\left(\frac{H}{L}\tau_{\alpha\alpha}^{[1]} + \frac{H^2}{L^2}\tau_{\alpha\alpha}^{[2]} + \ldots\right), \tag{2.1c}$$

$$\tau^* = \rho u_*^2 + \Delta\tau, \qquad \text{where } \Delta\tau = \rho u_*^2\left(\frac{H}{L}\tau^{[1]} + \frac{H^2}{L^2}\tau^{[2]} + \ldots\right), \tag{2.1d}$$

where the $\tau_{\alpha\alpha}$ are the total normal Reynolds stresses and the $T_{\alpha\alpha}$ are the normal Reynolds stresses in the approach flow. In most of what follows, the linear perturbations only are considered and the superscript [1] is omitted.

Before considering the governing equations and boundary conditions, a displaced coordinate system is introduced to ensure that at zeroth order the perturbed mean flow follows the topography near the surface and far above the surface the perturbations decay to zero. The displaced vertical coordinate, Z, is therefore defined to be proportional to the streamfunction of equivalent inviscid irrotational flow over the undulation. The displaced horizontal coordinate, X, is defined such that the overall coordinate system is orthogonal. Before defining explicitly the form of the transformation, we note the following simplification.

In the present analysis, only the linear perturbations to the flow are calculated, so

that Fourier transforms may be defined in the streamwise direction in order to solve the equations. The Fourier transform of, for example, the streamwise-velocity perturbation is defined by

$$\Delta u(s,z) = \int_{-\infty}^{\infty} \Delta u(x,z)\,\mathrm{e}^{-\mathrm{i}sx}\,\mathrm{d}x. \tag{2.2}$$

No special symbols are used for the transformed variables; when confusion may arise, they are distinguished by writing the argument list. An exception to this notational rule is the hill shape function, $f(x)$, whose transform is written

$$\tilde{f}(s) = \int_{-\infty}^{\infty} f(x)\,\mathrm{e}^{-\mathrm{i}sx}\,\mathrm{d}x. \tag{2.3}$$

At each wavenumber, s, a displaced and deformed set of coordinates is defined by

$$x = X - \frac{H}{L}\mathrm{i}\tilde{f}\tilde{F}(sZ), \qquad z = Z + \frac{H}{L}\tilde{f}\tilde{G}(sZ), \tag{2.4}$$

where $\tilde{G}$ and $\tilde{F}$ are defined by

$$\mathrm{d}^2\tilde{G}/\mathrm{d}Z^2 - s^2\tilde{G} = 0, \quad \tilde{F}' = G. \tag{2.5a}$$

Hence for a neutrally stratified flow that is unbounded in the vertical

$$\tilde{G} = \mathrm{e}^{-sZ}. \tag{2.5b}$$

In order that the normal velocity at the surface is zero, $\tilde{G}(0) = 1$.

In the linear approximation, the Fourier transforms defined with respect to X are equivalent to those defined in x (Belcher 1990†). Hence, to the linear approximation, the displaced coordinates are defined with respect to the Fourier transforms of the flow variables.

A crucial feature of the transformation to the displaced coordinate system is that the vertical velocity and Reynolds-stress perturbations change. Denoting the perturbations in the displaced coordinate system with subscript d, the vertical velocity transforms, to leading order in H/L, as

$$\begin{aligned} w(s,z) &= \mathrm{i}s\tilde{f}\tilde{G} + w_{\mathrm{d}}(s,Z) + O(H^2/L^2) \\ &\equiv w^{(0)}(s,z) + w_{\mathrm{d}}(s,Z) + O(H^2/L^2), \end{aligned} \tag{2.6}$$

which implies that $w^{(0)}$ is the inviscid irrotational vertical-velocity perturbation induced by the undulation. Under the transformation the Reynolds-stress components become

$$\tau_{xx} = \tau_{XX} - 2\mathrm{i}s\tilde{f}\tilde{G}, \quad \tau_{zz} = \tau_{ZZ} + 2\mathrm{i}s\tilde{f}\tilde{G}, \quad \tau = \tau_{\mathrm{d}} + \mathrm{i}s\tilde{f}\tilde{G}(T_{xx} - T_{zz})/\rho u_*^2. \tag{2.7}$$

These changes in the Reynolds stress arise from the kinematic effect of the rotation of the mean streamlines.

Solutions for the linear perturbations are obtained by transforming the governing equations into the displaced coordinate system. The details are laborious, but straightforward (see Belcher 1990), and the resulting solutions are equivalent to those obtained by HLR, who used a simpler discontinuous vertical coordinate. Hence the details of the coordinate transformation are not described here, although the subsequent extensions of the HLR analysis will be expressed in the displaced coordinate system (see also the Appendix).

† A copy can be obtained from the authors or the editorial office on request.

In non-dimensional form the Reynolds-averaged equations governing the leading-order perturbations to the flow in the displaced coordinates are

$$U\frac{\partial u_{\mathrm{d}}}{\partial X}+w_{\mathrm{d}}\frac{\mathrm{d}U}{\mathrm{d}Z}=-\frac{\partial p_{\mathrm{d}}}{\partial X}+\epsilon^2\left(\frac{\partial \tau_{\mathrm{d}}}{\partial Z}+\frac{\partial \tau_{XX}}{\partial X}\right), \tag{2.8a}$$

$$U\frac{\partial w_{\mathrm{d}}}{\partial X}=-\frac{\partial p_{\mathrm{d}}}{\partial Z}+\epsilon^2\left(\frac{\partial \tau_{\mathrm{d}}}{\partial X}+\frac{\partial \tau_{ZZ}}{\partial Z}\right), \tag{2.8b}$$

$$\frac{\partial u_{\mathrm{d}}}{\partial X}+\frac{\partial w_{\mathrm{d}}}{\partial Z}=0, \tag{2.8c}$$

where $\epsilon = u_*/U_0$ is the second basic small parameter of the problem, which is typically 0.03–0.07 in the atmosphere. (Note that the Reynolds number is assumed to be sufficiently large that the hill surface is aerodynamically rough and the viscous stresses can be neglected throughout the flow.) Equations (2.8*a*) and (2.8*b*) should each have two extra terms that arise from the coordinate transformation and involve the gradients of the unperturbed pressure and Reynolds-stress distributions. In the very deep boundary layers considered here, these terms are numerically small and have been neglected.

The boundary conditions on the leading-order perturbations are

$$u_{\mathrm{d}} = w_{\mathrm{d}} = 0 \quad \text{on} \quad Z = z_0/L \tag{2.8d}$$

and

$$u_{\mathrm{d}}, w_{\mathrm{d}}, p_{\mathrm{d}}, \tau_{\mathrm{d}} \to 0 \quad \text{as} \quad Z \to \infty. \tag{2.8e}$$

2.2. *Structure of the perturbed mean flow*

2.2.1. *Division into inner and outer flow regions*

The structure of the mean flow perturbations is now examined to determine the (dimensional) scale height, l, over which the Reynolds stresses significantly influence the dynamics of the mean flow perturbations. The scaling is carried out in terms of a small parameter that is defined as l/L by analogy with classical laminar boundary-layer theory. The $O(H/L)$ flow perturbations are now expanded in powers of l/L, so that for example

$$u_{\mathrm{d}} = u_{\mathrm{d}}^{(0)}(X,\zeta)+\frac{l}{2\kappa^2 L}u_{\mathrm{d}}^{(1)}(X,\zeta)+\ldots, \tag{2.9}$$

where $\zeta = ZL/l = Z^*/l$ is a stretched vertical coordinate. Then, at zeroth order, except very close to the surface (see §2.2.2 below), the inertial term in (2.8*a*) balances the pressure perturbation, i.e. at leading order (2.8*a*) becomes

$$U\frac{\partial u_{\mathrm{d}}^{(0)}}{\partial X}+\frac{\partial p_{\mathrm{d}}^{(0)}}{\partial X}=0. \tag{2.10a}$$

At first order in l/L, these terms are out of balance, and the residue is balanced by the leading-order perturbation shear-stress gradient. This first-order balance occurs at a height of order l if

$$\frac{\epsilon^2\,\partial\tau_{\mathrm{d}}^{(0)}/\partial Z}{U\,\partial u_{\mathrm{d}}^{(1)}/\partial X+\partial p_{\mathrm{d}}^{(1)}/\partial X}\sim\frac{\epsilon^2/l}{(\epsilon/\kappa)\ln(l/z_0)\{[(\epsilon/\kappa)\ln(l/z_0)]/L\}(l/L)}\sim 1, \tag{2.10b}$$

which reduces to $l\ln(l/z_0)\sim\kappa L$. It is convenient to fix the constant so that

$$l\ln(l/z_0)=2\kappa^2 L. \tag{2.11}$$

The small parameter for the inner region is then defined as

$$l/2\kappa^2 L = \ln^{-1}(l/z_0) = \epsilon/\kappa U(l). \tag{2.12}$$

(This is δ in the notation of HLR.) The scale height of the inner region is then $l \sim \epsilon L$. The parameter $U(l) = U_B(l)/U_B(h_m)$, which measures the shear across the middle layer, is of order one; it has, however, a numerically significant variation with ϵ:

$$U(l) \sim 1 + O(\epsilon \ln(1/\epsilon)) \quad \text{as} \quad \epsilon \to 0. \tag{2.13}$$

The flow domain is divided into two regions: $Z = O(1)$, the *outer region*, where the Reynolds stresses have an $O(\epsilon^2)$ effect on the mean flow (see §5.3 below), and $Z = O(\epsilon)$, the *inner region*, where the mean velocity perturbations are influenced by the perturbations to the shear stress at $O(\epsilon)$ (see also §5.1 below).

2.2.2. *Asymptotic structure of the outer and inner regions*

The arguments above show that in the outer region the perturbations are largely determined by inviscid dynamics. As in the well-established theory of perturbed laminar boundary layers (e.g. Smith *et al.* 1981), the perturbations to the flow in the outer region are inviscid, even though the unperturbed flow is determined by the viscous stresses for the laminar boundary layer or the Reynolds shear stress for the turbulent boundary layer; this point is elaborated in §5 when we analyse the distortion of turbulence in the outer region.

In the outer region (2.8) can be reduced to a single equation for w_d:

$$\frac{\partial^2 w_d}{\partial X^2} + \frac{\partial^2 w_d}{\partial Z^2} - \frac{U''}{U} w_d = O(\epsilon). \tag{2.14}$$

The $O(\epsilon)$ error is from the curvature terms; the neglected terms associated with the shear stress gradients are of second order in ϵ, if correctly calculated (see §5 below).

The height over which the shear term ($w_d U''/U$) is comparable with the horizontal gradient term ($\partial^2 w_d/\partial X^2$) depends on the length of the hill and the upwind velocity profile. If L is less than about 20% of the boundary-layer thickness, $U(z)$ is logarithmic up to a height $Z^* \sim L$. Then the ratio of these two terms is

$$\frac{(U_d''/U_d) w_d}{\partial^2 w_d/\partial X^{*2}} \sim \frac{L^2 \ln^{-1}(Z^*/z_0)}{Z^{*2}}. \tag{2.15}$$

This is $O(1)$ if $Z^* \sim h_m$, which implies that h_m is defined by the implicit equation

$$h_m \ln^{\frac{1}{2}}(h_m/z_0) = L, \tag{2.16}$$

so that

$$h_m = (\epsilon/\kappa)^{\frac{1}{2}} L. \tag{2.17a}$$

Conversely, if L is much greater than the boundary-layer thickness, h, (but still much less than h_*) then

$$h_m = h, \tag{2.17b}$$

since, by definition, there is no shear in the mean velocity profile outside the boundary layer.

Thus the outer region divides into two layers. In the *upper layer*, $Z = O(1)$, the shear in the unperturbed velocity is negligible and (2.14) reduces to the equation for potential flow. When $Z = O(h_m/L)$, the shear in the unperturbed velocity profile dominates the horizontal gradient. Then the perturbation velocities are inviscid but *rotational*. Following HLR, this is called the *middle layer*. The scale for the velocities is then the unperturbed boundary-layer value at the height h_m, $U_0 = U_B(Z^* = h_m)$.

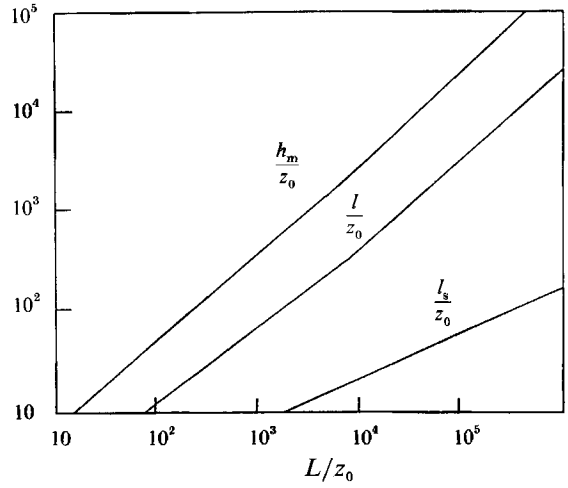

FIGURE 3. Variation of the heights of the asymptotic layers with L/z_0, where L is the length scale of the hill, and h_m, l and l_s refer to the middle layer, inner region (and shear-stress layer, SSL) and inner surface layer (ISL) respectively.

Near the surface ($Z = O(\epsilon)$) the pressure perturbation term balances the inertial stress terms at zeroth order and the shear stress is in balance with the residue of the inertial terms at first order. This is called the *shear-stress layer*, denoted (SSL). The detailed analysis of the (SSL) shows that the shear stress gradient solution diverges logarithmically at the surface (a point first made by Sykes 1980). It is therefore necessary to match the (SSL) solution with an even thinner layer, the *inner surface layer* (ISL). Across this layer, the perturbation shear stress is constant at zeroth order but its gradient changes by $O(1)$. HLR show that a characteristic height of the (ISL) is $l_s = (lz_0)^{\frac{1}{2}}$. The (ISL) is very thin; l_s can be related to the scale height of the inner region by

$$l_s = l\mathrm{e}^{-1/\epsilon}. \tag{2.18}$$

2.2.3. *Summary of assumptions, lengthscales and practical values*

The analytical theory is based on four assumptions. The first three have already been discussed and are (i) low slope, $H/L \ll 1$; (ii) $\epsilon = u_*/U_0 \ll 1$; and (iii) a rapidly varying pressure perturbation, $L \ll h_* = hu_*/U_0$, which ensures that the inner region lies well within the boundary layer. The fourth assumption is that the height of the hill is less than the scale height of the middle layer, $H \ll h_m$. This latter criterion is required so that the equations governing the flow perturbations in the middle layer may be linearized (see HLR). It is possible to derive nonlinear solutions for the middle layer which are valid when the linear solutions apply in the other layers (see HLR).

Given the above assumptions, the perturbed flow divides asymptotically into four layers. In the outer layer $Z = Z^*/L = O(1)$. In the middle layer $Z = O(h_m/L)$, which is of order $\epsilon^{\frac{1}{3}}$ when the approach flow is logarithmic throughout the middle layer. In the inner region $Z = O(l/L) = O(\epsilon)$ and, by assumption (iii), the upwind velocity profile is logarithmic in the inner region. In the inner surface layer $Z = O(l_s/L) = O(\mathrm{e}^{-1/\epsilon})$.

Graphs of h_m/z_0, l/z_0 and l_s/z_0 against L/z_0 are plotted in figure 3. Some practical values are: if $L = 250$ m and $z_0 = 0.1$ m, then $h_m \approx 95$ m, $l \approx 16$ m and $l_s \approx 1.3$ m, so that assumption (iv) requires that $H \ll 100$ m. A good working maximum value for the slope is $\frac{1}{3}$, so that, given $L = 250$ m, $H < 80$ m is required to keep the slope small.

2.3. *Drag calculation and asymptotic estimates*

The force on the hill surface, F_i, is computed by integrating (in the undisplaced coordinates) the normal component of the stress tensor, σ_{ij}, along the surface of the topography, viz.

$$\frac{F_i}{\rho U_0^2 L} = -\int \sigma_{ij} n_j \, \mathrm{d}S, \tag{2.19}$$

where $\boldsymbol{n}$ is the normal into the hill surface and is given by

$$\boldsymbol{n} = \left(\frac{H}{L} f', -1\right)\left(1 + O\left(\frac{H^2}{L^2}\right)\right). \tag{2.20}$$

Taking the horizontal component of (2.19) and substituting for the stress tensor, the perturbation drag force becomes

$$\frac{\Delta F}{\rho U_0^2 L} = \int_{Z=z_0} \left[\frac{H}{L}\epsilon^2 \tau^{[1]} + \frac{H^2}{L^2}\epsilon^2 \tau^{[2]}\right] \mathrm{d}x + \frac{H^2}{L^2}\int_{Z=z_0} (p^{[1]} - \epsilon^2 \tau_{xx}^{[1]}) f'\left(\frac{x}{L}\right) \mathrm{d}x + O\left(\frac{H^3}{L^3}\right). \tag{2.21}$$

The integrals are taken over one wavelength of periodic terrain, or from far upstream to far downstream for an isolated hill.

The integral of the linear stress term is zero. This result is obtained by integrating the linearized x-momentum equation, namely

$$\int_{x=-\infty}^{\infty}\int_{z'=z_0}^{Z} \frac{\partial \tau^{[1]}}{\partial z'} \mathrm{d}x \, \mathrm{d}z' = \int_{x=-\infty}^{\infty}\int_{z'=z_0}^{Z} \left[\frac{\partial p^{[1]}}{\partial x} + U\frac{\partial u^{[1]}}{\partial x} + w^{[1]} U'\right] \mathrm{d}x \, \mathrm{d}z'. \tag{2.22}$$

Integrating by parts and using continuity on the inertial terms gives

$$\int_{x=-\infty}^{\infty} (\tau^{[1]}(x,z) - \tau^{[1]}(x,z_0)) \, \mathrm{d}x = \int_{x=-\infty}^{\infty} w^{[1]}(x,z)\, U(z) \, \mathrm{d}x$$
$$+ \int_{z'=z_0}^{Z} [p^{[1]}(\infty,z') - p^{[1]}(-\infty,z') + 2u^{[1]}(\infty,z') - 2u^{[1]}(-\infty,z')] \, \mathrm{d}z'. \tag{2.23}$$

For an isolated hill, far upwind and far downwind the $p^{[1]}$ and $u^{[1]}$ perturbations are zero. For periodic terrain, they are periodic and so the last integrand on the right-hand side of (2.23) is zero. Then as $Z \to \infty$ the $w^{[1]}$ and $\tau^{[1]}$ perturbations tend to zero, so that

$$\frac{H}{L}\int \tau^{[1]}(x, z_0) \, \mathrm{d}x = 0. \tag{2.24}$$

These arguments show that the leading-order perturbation to the drag force is of second order in the slope of the topography, H/L, and that contributions arise from the components of the normal stress that are in phase with the slope of the undulation together with the mean value of the $O(H^2/L^2)$ shear-stress perturbation.

We focus on the force caused by the pressure perturbation, ΔF_p, (referred to as the pressure force) so that

$$\frac{\Delta F_p}{\rho U_0^2 L} = -\frac{H^2}{L^2}\int_{Z=z_0} p^{[1]} f' \, \mathrm{d}x. \tag{2.25}$$

The calculation of the pressure force now reduces to determining that part of the pressure that is in phase with the slope of the topography, i.e. out of phase with the elevation. In §3 we show that the out-of-phase pressure is of $O(\epsilon^2)$. hence for sinusoidal topography the integral over the pressure term in (2.25) reduces to

$$\Delta F_p = \rho U_0^2 4L \frac{H^2}{L^2}\left[\frac{\epsilon}{\kappa U(l)}\right]^2 \frac{1}{2} s \,\mathrm{Im}\,[\hat{\sigma}^{(2)}] + O(\epsilon^3)$$

$$= \rho u_*^2 \frac{H^2}{L^2} L \frac{2s}{\kappa^2 U^2(l)} \mathrm{Im}\,[\hat{\sigma}^{(2)}] + O(\epsilon^3), \tag{2.26}$$

where $\hat{\sigma}^{(2)}$ is the $O(\epsilon^2)$ pressure coefficient at the surface. Therefore the magnitude of the perturbation drag force is

$$\Delta F_p = O\left(\rho \frac{H^2}{L^2} L u_*^2\right). \tag{2.27}$$

2.4. *Equation governing the pressure perturbation*

Taking the divergence of the momentum equation and using the continuity equation leads to an equation for the pressure perturbation, which, in the displaced coordinate system, is

$$\frac{\partial^2 p_d}{\partial Z^2} - s^2 p_d = 2U' \mathrm{i}s w_d - \epsilon^2\left[-s^2 \tau_{XX} + \frac{\partial^2 \tau_{ZZ}}{\partial Z^2} + 2\mathrm{i}s \frac{\partial \tau_d}{\partial Z}\right]$$

$$- s^2 \tilde{f}\tilde{G}[2U'U - \epsilon^2(4\mathrm{i}s + 2s(T_{XX} - T_{ZZ}))]. \tag{2.28a}$$

Hence, when $Z = Z^*/L = O(1)$, the equation (2.28*a*) for the pressure is elliptic. The group of terms on the right-hand side in the bracket multiplied by $\tilde{f}\tilde{G}$ arise from the transformation into the displaced coordinate system and are proportional to the curvature of the streamlines, $s^2\tilde{f}$.

Since the flow in the upper layer is potential flow (see HLR), the boundary condition on the presure perturbation at the bottom of the upper layer, where $Z \sim h_m/L$, shows that

$$\frac{\mathrm{i}s}{L} p_d\left(Z \sim \frac{h_m}{L}\right) = \frac{\partial w}{\partial Z}\left(Z \sim \frac{h_m}{L}\right), \tag{2.28b}$$

where w is the vertical velocity perturbation in the Cartesian frame.

Equations (2.28) show that an asymmetric pressure perturbation, which develops in the upper layer, can arise from three sources: (i) an asymmetric flow in the layers below the upper layer, which affect the upper-layer pressure perturbation through the boundary condition (2.28*b*); (ii) an asymmetric vertical velocity perturbation that is generated within the upper layer; or (iii) an asymmetric Reynolds stress perturbation that is generated within the upper layer.

3. Analytical solutions for the effect of non-separated sheltering

The boundary condition on the pressure, (2.28*b*), has an asymmetric component from the matching with the inner region and leads to the dominant contribution to the asymmetric pressure. It is termed non-separated sheltering. The HLR analysis is now extended to calculate this term.

The solutions derived by HLR (the full solutions are listed in the Appendix) for the

perturbations in the inner region show that the streamwise velocity perturbation is not exactly in phase with the undulation. The first two terms in the ϵ-expansion (2.9) are

$$\left.\begin{aligned} u_{\mathrm{d}}^{(0)}(s,\zeta) &= -\frac{\hat{\sigma}^{(0)}}{U(l)} \\ u_{\mathrm{d}}^{(1)}(s,\zeta) &= -\frac{\hat{\sigma}^{(0)}}{U(l)}\{1-\ln\zeta-4K_0[2(\mathrm{i}s\zeta)^{\frac{1}{2}}]\}. \end{aligned}\right\} \tag{3.1}$$

Here $\hat{\sigma}^{(0)} = -s\tilde{f}$ is the leading-order (in ϵ) surface pressure perturbation and $(1-\ln\zeta)$ is the local form of the middle-layer solution (recall that $\zeta = Z^*/l$). K_0 is the modified Bessel function (e.g. Abramowitz & Stegun 1972), which arises due to the balance in the shear-stress layer (SSL) between $U(l)\,\partial u_{\mathrm{d}}/\partial X$ and $\partial \tau_{\mathrm{d}}/\partial Z$ (together with the mixing-length formula, which is discussed in §5.2). Furthermore, K_0 has real and imaginary parts so that it has components both in and out of phase with the undulation. At the top of the inner region, as $\zeta \to \infty$, however, $K_0 \to 0$, so that there is no asymmetry in the horizontal velocity above the inner region at this order.

Using the continuity equation (2.8*c*), the $O(\epsilon^2)$ vertical velocity is given by

$$w_{\mathrm{d}}^{(2)}(s,\zeta) = -\frac{2\kappa^2\hat{\sigma}^{(0)}}{U(l)}\left[\mathrm{i}s\zeta(\ln\zeta-2)+4\left(\tfrac{1}{2}+\zeta\frac{\partial K_0}{\partial\zeta}\right)\right]. \tag{3.2}$$

The first set of terms, which are part of the inviscid (middle layer) component of the perturbation, are in phase with the slope of undulation and are not further considered. The second set of terms, however, are forced by the asymmetric part of the $O(\epsilon)$ streamwise velocity perturbation; the constant $\frac{1}{2}$ is required to ensure that the vertical velocity is zero at the bottom of the (SSL), to match with the (ISL) where $\zeta \sim l_{\mathrm{s}}/l$. The higher-order terms $u_{\mathrm{d}}^{(2)}$ and $w_{\mathrm{d}}^{(3)}$ have been derived by Belcher (1990) and compared in detail with numerical and experimental results by Weng *et al.* (1991). Examples of comparisons between numerical results and the first- and second-order analytical solutions are given in figures 4(*a*) and 4(*b*). Note that the analytical solutions for the (SSL) are asymptotic series and, for finite values of ϵ, the solution for u_{d} does not equal zero as $\zeta \to 0$. However, the (ISL) solutions satisfy the no-slip surface condition and match with u_{d} in the (SSL) as $\epsilon \to 0$ (see Belcher & Hunt 1993*b*). Weng *et al.* (1991) have suggested a heuristic, uniformly valid, formula that is continuous for finite ϵ and satisfies the boundary conditions.

At the top of the inner region, as $\zeta \to \infty$, the leading-order vertical-velocity perturbation that is in phase with the undulation is obtained from (3.2), which, on using the limit $\zeta\,\partial K_0/\partial\zeta \to 0$ as $\zeta \to \infty$, becomes

$$\mathrm{Re}\,[w_{\mathrm{d}}^{(\mathrm{SSL})}] \sim -\frac{2\epsilon^2}{U^3(l)}2\hat{\sigma}^{(0)} \quad \text{as} \quad \zeta \to \infty. \tag{3.3}$$

In the following, $\mathrm{Re}\,[w_{\mathrm{d}}^{(\mathrm{SSL})}]$ denotes the real part of the (SSL) vertical-velocity perturbation in the limit $\zeta \to \infty$. This shows that at $O(\epsilon^2)$ there is an out-of-phase displacement of the streamlines at the top of the inner region. This we term *non-separated sheltering*, because it is related to Jeffreys' (1925) 'sheltering hypothesis', which he suggested to account for the growth of surface waves on water due to the blowing of the wind. He supposed that the air flow separates at the crest of the wave and subsequently re-attaches downstream. In the present study the flow is not separated, but the asymmetric displacement of the streamlines about the undulation is due to thickening of the boundary layer on the leeside of the undulation (which may be regarded as the initial stages of separation).

In order to calculate the asymmetric pressure boundary condition on the upper layer, it is necessary to examine how this out-of-phase vertical velocity perturbation is transmitted through the middle layer. In this section, the non-separated sheltering effect only is considered, so that it is not necessary to consider any asymmetries generated within the middle layer (these are dealt with in §6.2 below). Hence (3.3) must match with the solution to the homogeneous equation governing the middle-layer perturbations. In the middle layer, where the horizontal gradient $\partial^2 w_d/\partial X^2$ is much smaller than the shear term, $w_d U''/U$, the equation governing the vertical velocity perturbations is

$$\frac{\partial^2 w_d}{\partial Z^2} - \frac{U''}{U} w_d = 0. \tag{3.4}$$

The leading-order vertical-velocity perturbation in the middle layer that is in phase with the undulation may then be written using the Heisenberg solution

$$\mathrm{Re}[w_d] \sim B_0 U + C_0 U \int^{\hat{Z}} \frac{\mathrm{d}Z'}{U^2(Z')}, \tag{3.5}$$

where $\hat{Z} = Z^*/h_m = Z/\epsilon^{\frac{1}{3}}$. Taking the limit $\hat{Z} \to 0$ and rewriting in (SSL) variables, the form of (3.5) that must match with (3.3) is

$$\mathrm{Re}[w_d] \sim B_0 U(l) + C_0 \frac{2\kappa}{U^2(l)} \epsilon^{\frac{1}{3}} \zeta + O(\epsilon) \quad \text{as} \quad \hat{Z} \to 0 \tag{3.6}$$

since $l/h_m = 2\kappa\epsilon^{\frac{1}{3}}/U(l)$. Hence (3.3) and (3.6) match if

$$B_0 = \frac{2\epsilon^2}{U^4(l)} 2\hat{\sigma}^{(0)} = \frac{1}{U(l)} \mathrm{Re}[w_d^{(\mathrm{SSL})}]. \tag{3.7}$$

The constant C_0 cannot be determined until the outer-layer solution has been calculated.

At the top of the middle layer, as $\hat{Z} \to \infty$, (3.5) becomes

$$\mathrm{Re}[w_d] \sim \frac{1}{U(l)} \mathrm{Re}[w_d^{(\mathrm{SSL})}], \tag{3.8}$$

since by definition $U(h_m) = 1$. Equation (3.8) must match with the outer layer. The homogeneous equation governing the vertical-velocity perturbation in the outer region is Laplace's equation, so that the solution is

$$\mathrm{Re}[w_d] = \frac{1}{U(l)} \mathrm{Re}[w_d^{(\mathrm{SSL})}] \tilde{G} + O(\epsilon^{\frac{1}{3}}), \tag{3.9}$$

where $\tilde{G}$ is defined by (2.5*a*). Finally, the continuity and X-momentum equations show that

$$\mathrm{Im}[p_d] = -\mathrm{Im}[u_d] = -\mathrm{i}\frac{1}{U(l)} \mathrm{Re}[w_d^{(\mathrm{SSL})}] \tilde{G}', \tag{3.10}$$

where Im denotes the imaginary part.

Hence the thickening of the boundary layer downwind of the hill crest leads to the outer-region flow being slightly out of phase with the topography. This leads to an out-of-phase surface pressure equal to

$$\mathrm{Im}[p_d(s, z_0)] = -\mathrm{i}\frac{1}{U(l)} \mathrm{Re}[w_d^{(\mathrm{SSL})}] \tilde{G}'(0) = -\frac{4\epsilon^2}{U^4(l)} \mathrm{i}s\tilde{f}\tilde{G}'(0). \tag{3.11}$$

3.1. *An alternative derivation*

The non-separated sheltering mechanism leads to the largest contribution to the asymmetric pressure and so it is instructive to consider in detail how it arises. By continuity, the vertical-velocity perturbation at the top of the inner region that is in phase with the undulation is given by

$$\mathrm{Re}\,[w_{\mathrm{d}}^{(\mathrm{SSL})}(\zeta\to\infty)] = -\frac{2\kappa\epsilon}{U(l)}\mathrm{Re}\left[\int_0^\infty \mathrm{i}s u_{\mathrm{d}}\,\mathrm{d}\zeta\right]. \tag{3.12}$$

Using the linearized X-momentum equation,

$$-\mathrm{Re}\,[\mathrm{i}s u_{\mathrm{d}}] = \mathrm{Re}\left[\frac{w_{\mathrm{d}}}{2\kappa^2\zeta}+\frac{\mathrm{i}s}{U(l)}u_{\mathrm{d}}\frac{\epsilon}{\kappa}\ln\zeta+\frac{\mathrm{i}s}{U(l)}p_{\mathrm{d}}-\epsilon\frac{\partial\tau_{\mathrm{d}}}{\partial\zeta}\right]. \tag{3.13}$$

The first three terms are of $O(\epsilon^2)$ and the final term is of $O(\epsilon)$. Hence, the leading-order contribution to the asymmetric vertical-velocity perturbation is

$$\mathrm{Re}\,[w_{\mathrm{d}}^{(\mathrm{SSL})}(\zeta\to\infty)] = -\frac{\epsilon^2}{U(l)}\mathrm{Re}\left[\int_0^\infty\frac{\partial\tau_{\mathrm{d}}}{\partial\zeta}\mathrm{d}\zeta\right]+O(\epsilon^3) = -\frac{\epsilon^2}{U(l)}\mathrm{Re}\,[\tau_{\mathrm{d}}(\zeta\to\infty)-\tau_{\mathrm{d}}(0)]. \tag{3.14}$$

The asymmetric surface pressure induced by the non-separated sheltering may hence be written

$$\mathrm{Im}\,[p_{\mathrm{d}}] = \mathrm{i}\frac{\epsilon^2}{U^2(l)}\mathrm{Re}\,[\tau_{\mathrm{d}}(\zeta\to\infty)-\tau_{\mathrm{d}}(0)]\,G'(0) = -\frac{4\epsilon^2}{U^4(l)}\mathrm{i}s\tilde{f}\tilde{G}'(0). \tag{3.15}$$

This shows that the leading-order asymmetry in the flow within the (SSL) occurs through the balance, in the X-momentum equation, between the inertial term, $U(l)\,\partial u_{\mathrm{d}}/\partial X$, and the Reynolds shear-stress gradient, $\partial\tau_{\mathrm{d}}/\partial Z$. The important feature of this result is that it shows that the out-of-phase displacement of the streamlines is dependent on the leading-order shear-stress perturbation that is in phase with the topography. With the mixing-length turbulence model, the shear-stress perturbation that is in phase with the undulation is in good agreement with the numerical calculations, §5.2. Hence the present calculation gives a good quantitative value of the leading-order pressure asymmetry induced by the non-separated sheltering effect.

4. The numerical model

We now present and analyse results of numerically integrating the full nonlinear momentum equations with (i) a mixing-length model for the shear stress throughout the perturbed flow and (ii) a 'second-order'-closure model for the turbulent stresses. These results show the strengths and limitations of these two levels of turbulence model and are used to establish theoretical scaling arguments (§5) to describe the changes to the turbulence.

The underlying physical assumption of a mixing-length model of the Reynolds shear stress is that the turbulence is in a local equilibrium where the production of turbulent kinetic energy balances, at leading order, its dissipation (Townsend 1961). Equivalently, the mixing-length model is appropriate only when the timescale of the turbulent eddies is much less than the timescale imposed by the perturbation. As we show in §5 below, these criteria are satisfied only in the inner region. Therefore to assess the limitations of the simple mixing-length model and to compute the entire flow

with one turbulence model that is valid everywhere (even if, inevitably, it is approximate), it is necessary to use a more general model that incorporates the effects of advection, pressure redistribution and turbulent transport of turbulent energy, such as the second-order-closure model of Launder, Reece & Rodi (1975) (referred to herein as LRR). We present the results of computations performed using both models.

4.1. *The mixing-length turbulence model*

In the mixing-length model of the Reynolds streses (as used by Taylor & Gent 1974 and later authors), an eddy-viscosity hypothesis is first made to relate the Reynolds stresses to the mean flow:

$$\tau_{ij} = \nu_{\mathrm{t}}\left(\frac{\partial U_i}{\partial x_j}+\frac{\partial U_j}{\partial x_i}\right). \tag{4.1}$$

The turbulent 'viscosity', ν_{t}, is then related to the mean flow by

$$\nu_{\mathrm{t}} = l_{\mathrm{m}}^2\left|\frac{\partial U_i}{\partial x_j}+\frac{\partial U_j}{\partial x_i}\right|, \tag{4.2}$$

and the mixing length l_{m} is specified by

$$1/l_{\mathrm{m}} = 1/\kappa z + 1/\lambda_{\mathrm{b}}, \tag{4.3}$$

where the von Kármán constant, κ, is taken to be 0.4, and λ_{b} is an empirically determined length of about one tenth the boundary-layer depth, but which depends on the flow since it determines l_{m} towards the edge of the boundary layer (where the mixing-length model is not accurate).

4.2. *Second-order-closure model for the turbulence*

The Reynolds-stress equation, in a flow that is steady in the mean, takes the form

$$U_k\frac{\partial \tau_{ij}}{\partial x_k} = P_{ij}+\Pi_{ij,1}+\Pi_{ij,2}+D_{ij}+\varepsilon_{ij}. \tag{4.4}$$

The term on the left-hand side of (4.4) represents the advection of the Reynolds stresses by the mean velocity, the first term on the right-hand side of (4.4) is the production of Reynolds stress by the mean flow, the second and third are the linear and nonlinear pressure redistribution terms, the fourth, the diffusion of Reynolds stress by the fluctuating velocity and by molecular viscosity, and the fifth, the rate of dissipation of the turbulence stresses by molecular viscosity.

The production terms are linear in the Reynolds stress and require no modelling. They are given by

$$P_{ij} = -\left(\tau_{ik}\frac{\partial U_j}{\partial x_k}+\tau_{jk}\frac{\partial U_i}{\partial x_k}\right), \quad P_r = \tfrac{1}{2}P_{kk}, \tag{4.5}$$

The anisotropic rate of dissipation, ε_{ij}, is approximated by the isotropic form, $\frac{2}{3}\varepsilon\delta_{ij}$, which is determined from another approximate transport equation:

$$u_k\frac{\partial \varepsilon}{\partial x_k} = -c_\varepsilon\frac{\partial}{\partial x_j}\left(\frac{k}{\varepsilon}\tau_{jk}\frac{\partial \varepsilon}{\partial x_k}\right)+c_{\varepsilon 1}\tau_{jk}\frac{\varepsilon}{k}\frac{\partial U_j}{\partial x_k}-c_{\varepsilon 2}\frac{\varepsilon^2}{k}, \tag{4.6}$$

where $k = -\frac{1}{2}\tau_{ii}$, see LRR. There are two pressure strain terms in (4.4), the slow, 'return to isotropy' term, which is modelling according to the suggestion of Rotta, namely

$$\Pi_{ij,1} = c_1(\varepsilon/k)\,(\tau_{ij}-\tfrac{2}{3}k\delta_{ij}). \tag{4.7}$$

The rapid term, $\Pi_{ij,2}$, models the redistribution of the stress due to the interaction of the stresses with the mean flow. This term gives rise to the changes induced in the Reynolds stresses due to the rapid distortion in the outer region. Furthermore, it is important to model this term correctly to evaluate the effects on the perturbations of mean streamline curvature and anisotropy of the turbulence in the approach flow (Zeman & Jensen 1987).

If the turbulence is assumed homogeneous, and if the second spatial gradients of the mean flow are assumed small, then $\Pi_{ij,2}$ is dependent only on the local and instantaneous strain and second-order turbulence moments. Although this term should also be dependent on the history of the strain (Hunt 1978), most present second-order models assume a linear dependence on τ_{ij} and the local strain rate $\partial U_i/\partial x_j$. We use the proposal of LRR, namely

$$\Pi_{ij,2} = -\frac{c_2+8}{11}(P_{ij}-\tfrac{2}{3}P_r\delta_{ij})+\frac{30c_2-2}{55}k\left(\frac{\partial U_i}{\partial x_j}+\frac{\partial U_j}{\partial x_i}\right)-\frac{8c_2-2}{11}(Q_{ij}-\tfrac{2}{3}P_r\delta_{ij}). \quad (4.8)$$

The coefficients of each of the bracketed terms is related to the single constant, c_2, using the symmetry conditions of $\Pi_{ij,2}$, and linearizing in the anisotropy (see LRR). Q_{ij} is defined by

$$Q_{ij} = -\left(\tau_{ik}\frac{\partial U_k}{\partial x_i}+\tau_{ki}\frac{\partial U_k}{\partial x_i}\right). \quad (4.9)$$

The general expression for the pressure strain correlation shows that there are surface integral terms which become important near rigid boundaries (see e.g. LRR). To predict correct stress ratios (even in an equilibrium boundary layer) extra 'wall' terms are included in the rapid pressure strain. Specific forms for these correction terms have been suggested, but a careful analysis of the resulting stress equations, in the near-wall limit, for an equilibrium boundary layer shows that the equations have a non-unique root (Newley 1986). If the ratios of the Reynolds-stress components are assumed to have their correct values at the surface, then the vertical profile of the shear stress has unphysical fluctuations of order 15%, which have the same magnitude as the perturbations induced by the topography. The failure of these models compelled us to ignore wall correction terms at the expense of predicting stress ratios at the surface that do not agree with atmospheric observations. Zeman & Jensen (1987) avoided wall correction terms by using the more general $\Pi_{ij,2}$ model of Zeman & Tennekes (1975), which contains more empirical constants than the LRR model. These extra constants are adjusted so that the near-surface stress ratios of an equilibrium boundary layer agree with the observed atmospheric data.

Lastly, the term representing transport of Reynolds stress due to the fluctuating velocity is modelled by a generalized gradient transfer model

$$T_{ij} = -c_s\frac{\partial}{\partial x_k}\left[\frac{k}{\varepsilon}\left(\tau_{im}\frac{\partial \tau_{jk}}{\partial x_m}+\tau_{jm}\frac{\partial \tau_{ki}}{\partial x_m}+\tau_{km}\frac{\partial \tau_{ij}}{\partial x_m}\right)\right]. \quad (4.10)$$

The empirical constants in the model were taken to be $c_1 = 1.5$, $c_2 = 0.4$, $c_s = 0.11$, $c_\varepsilon = 0.281$, $c_{\varepsilon 1} = 1.44$, $c_{\varepsilon 2} = 1.9$.

4.3. *Solution procedure*

The equations (4.1) and (4.2) were solved by first mapping the flow domain, $z_s = Hf(x^*/L)$ to $z^* = D$, into a rectangle, by defining a vertical coordinate transformation, $\tilde{z} = D(z^*-H)/(D-H)$. The equations were then transformed into

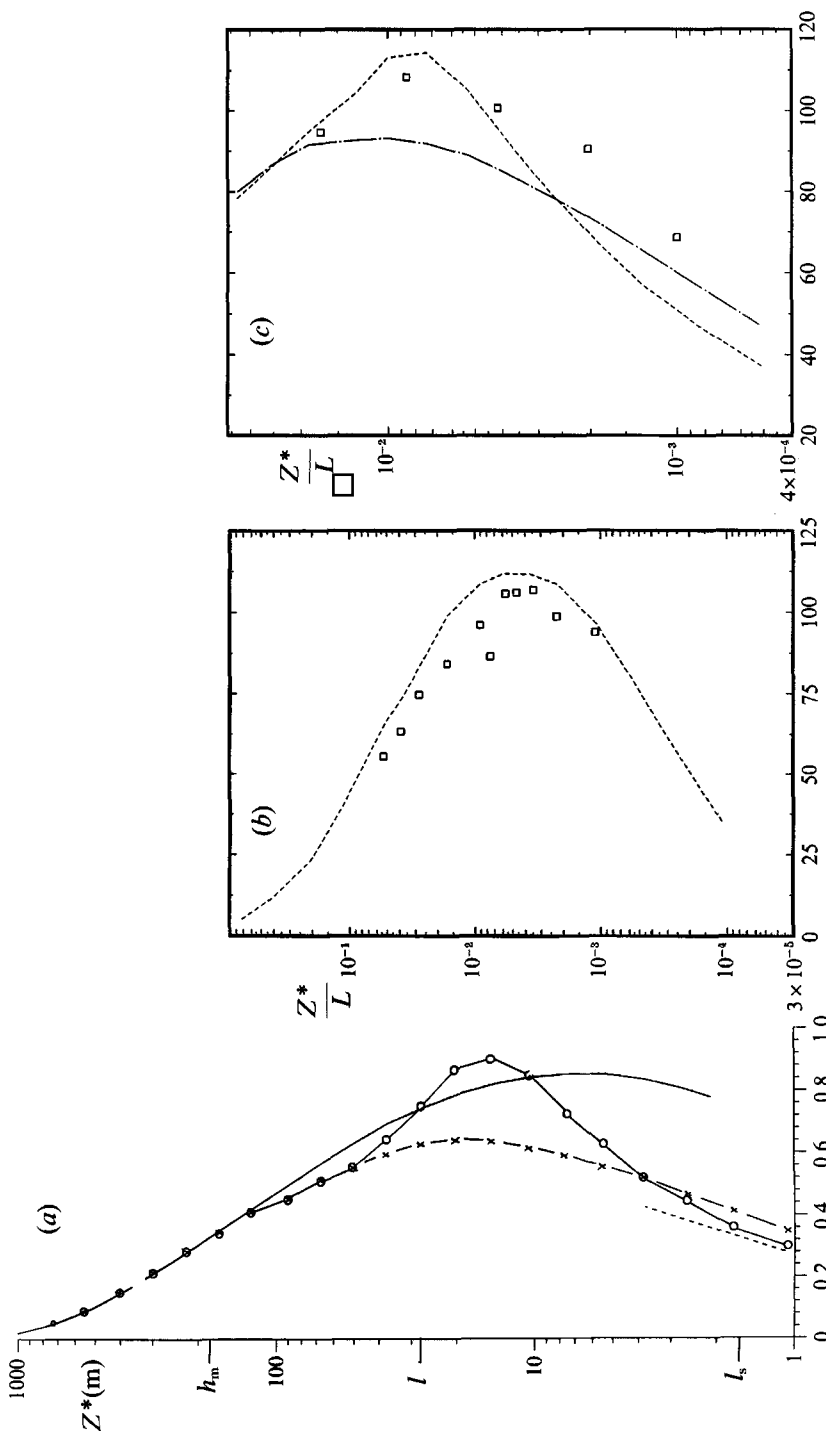

FIGURE 4. (*a*) Comparison of the streamwise-velocity perturbation at the crest of sinusoidal topography (with $H/L = 0.04$ and $z_0/L = 2\times10^{-4}$) calculated using the asymptotic theory and the results computed using the second-order-closure model: ——, analytic solution for the middle layer and (SSL) to $O(\epsilon)$; – – –, analytic solution for the (ISL) to $O(\epsilon)$; —○—, results computed using the second-order-closure model; —×—, results computed using the mixing-length model. (*b*) The streamwise-velocity perturbation (normalized on $u_* H/L$) at the summit of Askervein hill (which is described by $f(x) = (1+x^2)^{-1}$, $H/L = 0.46$ and $z_0/L = 3\times10^{-5}$) calculated using the asymptotic theory and the results measured experimentally (reported in Zeman & Jensen 1987): – – –, analytic solution for the middle layer and (SSL) to $O(\epsilon)$; □, experimental measurements. (*c*) Comparison of the streamwise-velocity perturbation (normalized on $u_* H/L$) measured by Mason (1986*b*) at the summit of Nyland hill (which has $H/L = 0.4$ and $z_0/L = 6\times10^{-5}$) and the values computed using the numerical models with a hill defined by (4.13) with $H/L = 0.08$ and $z_0/L = 5\times10^{-5}$: – – –, numerical results using the second-order-closure model; – · –, numerical results using the mixing-length model; □, experimental measurements.

this non-orthogonal system. To compute the fine details of the flow near the surface, a variable mesh size was used (the ratio of adjacent mesh points was approximately 1.3) and the position of the first grid point was selected as ~ 0.1 m (i.e. about $10z_0$); 32 grid points were used in the vertical and 16 in the horizontal direction (which was regular). In order to achieve the steady solution, the flow was started from rest and the solution integrated forward in time. The time step, Δt, was determined by the smallest important timescale of the problem $\Delta z/(4u_*)$ (so that when the geostrophic wind $U_G = 10\ \mathrm{ms}^{-1}$, Δt was taken to be 0.02 s). Then steady solutions were obtained after ten times the travel time across the terrain. Hence the number of time steps required was 10^5. This led to a convergence time of about 17 h on the IBM 3081 computer at the UK Met. Office (subsequent reprogramming has reduced the convergence time to about 7 h, P. J. Mason & N. Wood, personal communication). The usual grid refinement tests were made, and the solution changed by less 1%. All details of the numerical procedure may be found in Newley (1986).

Solutions to the model were computed for two hill shapes: periodic, sinusoidally varying undulations,

$$f = 1 + \sin(\tfrac{1}{2}\pi x); \tag{4.11}$$

and an isolated hill,

$$f = \begin{cases} 1 + \cos(\tfrac{1}{2}\pi(x - x_c)) & \text{if} \quad x_c - 2 < x < x_c + 2, \\ 0 & \text{otherwise}, \end{cases} \tag{4.12}$$

where, in each case, x is made dimensionless with L, the half-length of the hill.

Profiles of the mean velocity and shear-stress perturbations for the two computational models, together with some comparisons, are shown in figures 4, 7, and 8.

Figure 4(*a*) shows a comparison of the velocity profile at the crest of sinusoidal terrain ($H/L = 0.04$) computed using the linear model and the numerical results. The maximum value of the velocity perturbation is in good agreement with the second-order-closure results, although the height of the maximum is slightly lower according to the theory. At larger slopes, the linear model still gives reasonable predictions of the mean velocity at the crest as is shown in figure 4(*b*), where $H/L \approx 0.5$. Figure 4(*c*) shows a comparison between the results of the numerical model and the field data measured at Nyland hill (Mason 1986*b*). The numerical results are for isolated terrain with $H/L = 0.08$, whereas Nyland hill has $H/L \approx 0.4$. This graph serves to check the linear approximation: the velocity perturbations are plotted as $\Delta u/(u_* H/L)$, hence, if the linear approximation and the second-order closure model were perfect, the results would collapse. The graph shows that the maximum speed-up is calculated reasonably well by the LRR-model given this linearization. The poorer agreement near the surface is explained, at least partly, by the linear assumption being used for a relatively large slope.

5. Perturbations to the turbulence structure

5.1. *Division of the flow into inner and outer regions*

The acceleration and deceleration of the mean flow changes the structure of the turbulence through two processes. Firstly, the mean velocity gradients strain the turbulent eddies. The timescale, T_D, of these straining distortions is the time taken for an eddy to be advected by the mean flow over the distance L, i.e.

$$T_D = \frac{L}{U_B(Z)} = \frac{L}{(u_*/\kappa)\ln(Z^*/z_0)}, \tag{5.1}$$

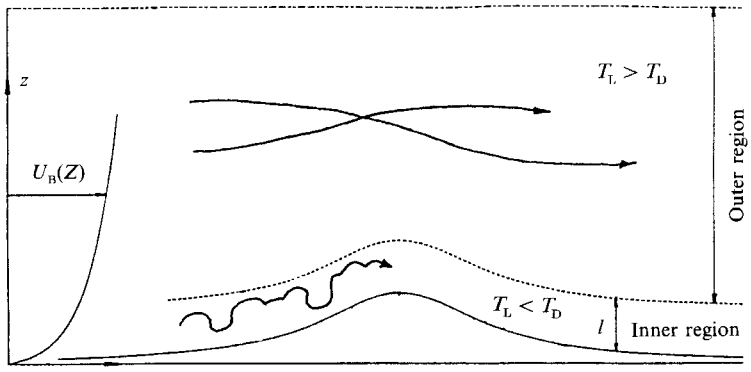

FIGURE 5. Schematic of typical particle paths in the inner and outer region.

assuming the approach flow profile is logarithmic. Secondly, the structure of the turbulence is modified by the changes in the interactions between the eddies, whose significance depends on the time taken for larger eddies to strain smaller eddies, which thence become decorrelated. This gives a second fundamental timescale, T_L. Near the surface in an equilibrium boundary layer, the high shear and the blocking effect of the wall determine the strain rates and scales of the energy-containing eddies, which determine the dissipation rates. These are of the same order as those of the vertical components of the turbulence; close to a rigid boundary, the timescale of the horizontal fluctuations is determined by the large-scale motions in the bulk of the flow (the inactive motions of Bradshaw 1967 and Townsend 1961). From measurements and direct numerical simulations, it is found that the integral lengthscale, $L_x^{(w)}$ and Lagrangian time scale, T_L, may be related approximately by

$$T_L \sim \frac{\varepsilon}{\overline{u'^2}+\overline{v'^2}+\overline{w'^2}} \sim \frac{L_x^{(w)}}{(\overline{w'^2})^{\frac{1}{2}}} \sim \frac{\kappa Z^*}{u_*}. \tag{5.2}$$

Thus, near the surface, where $T_L < T_D$, the eddies decorrelate and lose energy on a timescale less than the distortion time, T_D, so that the production of energy has to balance its dissipation and the turbulence is in local equilibrium (except for the largest horizontal motions, Mason & King 1985).

At a (dimensional) distance l from the surface, these two timescales are of the same order of magnitude. l is defined implicitly by

$$l \ln (l/z_0) \sim L. \tag{5.3}$$

Thus the height l separates the perturbed flow into two regions (figure 1). Above this height, $T_L > T_D$ and the timescale of the interactions is small compared with the time it takes for the flow to pass over the hill. Note that, since $L_x^{(w)} \sim 0.4Z^*$, the energy-containing eddies are only weakly affected by the blocking effect of the wall; this is to be contrasted with the case of thermal convection, where the blocking effect is of central importance (Hunt 1984).

This division of the perturbed flow into inner and outer regions is shown schematically from a Lagrangian point of view in figure 5. In the outer region the particle paths are smoothly undulating curves, because the advection by the mean flow is more rapid than the eddying motions; whereas, in the inner region, the path of a fluid element is more random since the turbulent advection occurs on a shorter timescale than the mean flow advection.

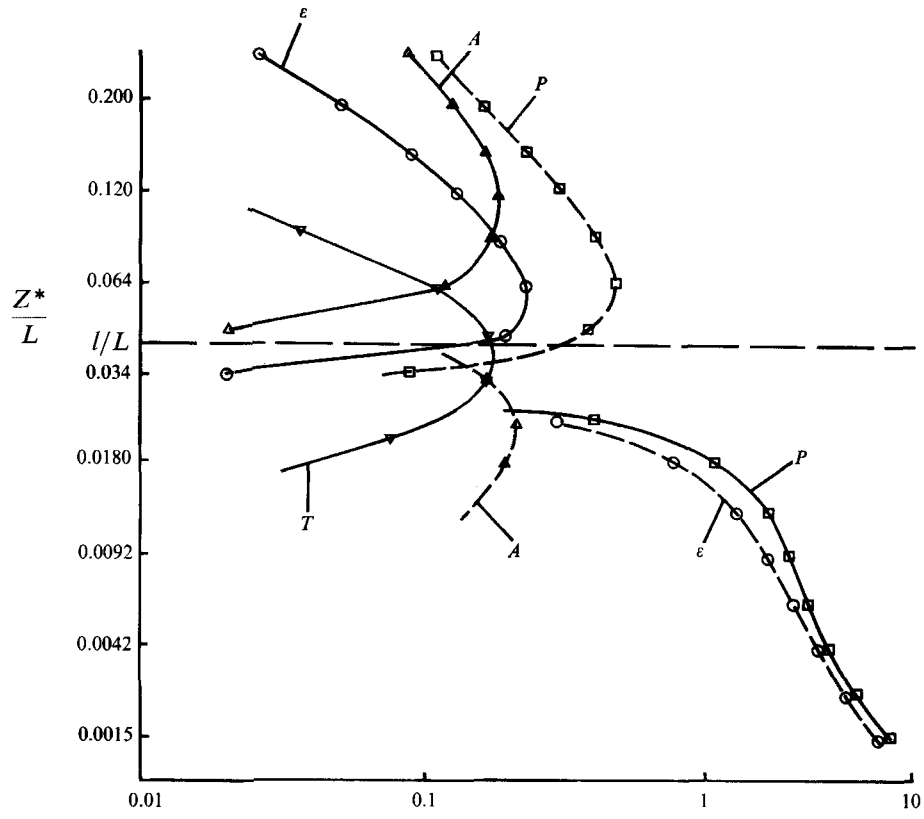

FIGURE 6. Balance of terms in the turbulent kinetic energy equation (normalized on u_*^3/L) integrated from far upstream to the crest of an isolated hill (defined according to the parameters of the numerical results in figure 4*c*): *P*, integrated production rate; *A*, integrated advection; *T*, integrated transport; ε, integrated dissipation rate. Solid lines denote positive quantities and dashed negative.

Figure 6 shows the balance of terms in the equation for the perturbed turbulent kinetic energy for flow over an isolated hill obtained from the results of the numerical model with the LRR model for the Reynolds stresses. In order to show the mechanisms through a range of the flow, each of the terms has been integrated over X^* from far upstream to the summit of the hill. Noting the logarithmic scales, the results show how in the lower part of the inner region ($Z^* < \frac{1}{2}l$) the production and dissipation processes dominate, with the advection term becoming significant at $Z^* \approx \frac{1}{2}l$ and the transport term becoming comparable at $Z^* \approx l$. In the outer region the advection and production terms dominate: when $Z^* \approx 4l$ they are approximately double ε. The results shown in figure 6 also show that, according to the second-order closure model, at the height $Z^* \approx l$, all the terms in the turbulent kinetic energy equation are significant (see also Zeman & Jensen 1987). The curvature of the mean streamlines also has an effect at this level, but is not shown in figure 6. These conclusions are consistent with field and laboratory observations (see §5.3.1 below).

5.2. *Inner region*

In the inner region, as Z^*/l decreases, the eddy–eddy interactions become more important than the irrotational straining by the distorted mean flow and the turbulence adjusts to the local mean velocity gradient (Townsend 1961). Hence the perturbation shear stress may be described asymptotically by the mixing-length model.

In the analytical model the shear stress is modelled by a mixing-length model throughout the depth of the inner region, so that

$$\frac{\Delta\tau}{\rho u_*^2} = 2\kappa^2 \frac{U_0}{u_*} Z^* \frac{\partial}{\partial Z^*}\left(\frac{\Delta u}{U_0}\right). \tag{5.4}$$

This model is not used, however, in the outer region (see the further discussion below).

Townsend (1976) reports that in the local equilibrium layer near a rigid boundary the ratios of the stress components are approximately the same for a variety of different external flows. Since the flow in the perturbed boundary layer is in local equilibrium close to the wall, these ratios remain the same, which implies that

$$\Delta\overline{u'w'}/\overline{u'w'} = \Delta\overline{u'^2}/\overline{u'^2} = \Delta\overline{v'^2}/\overline{v'^2} = \Delta\overline{w'^2}/\overline{w'^2}, \tag{5.5a}$$

where $-\overline{u_i' u_j'} = \tau_{ij}/\rho$. Commonly quoted values for these ratios in high Reynolds number (e.g. atmospheric) flows are

$$\alpha = -\overline{u'^2}/\overline{u'w'} \approx 6.3, \quad \beta = -\overline{v'^2}/\overline{u'w'} \approx 4.5, \quad \gamma = -\overline{w'^2}/\overline{u'w'} \approx 1.7. \tag{5.5b}$$

The constancy of these ratios has been used in many models of turbulent boundary layers that are perturbed on long and short lengthscales. (e.g. Bradshaw, Ferris & Atwell 1967 and Townsend 1972). The field data of Bradley (1980) and the results obtained numerically using the LRR (Newley 1986) and Zeman & Tennekes (Zeman & Jensen 1987) turbulence models are all consistent with (5.5*a*). As explained in §4.2, the values of α, β and γ obtained with the results of Newley's computations are not the same as the atmospheric observations.

The detailed analysis using the mixing length model (see HLR) shows that, near the surface ($Z^* < \frac{1}{3}l$), Δu varies approximately logarithmically so that

$$\partial\Delta u/\partial Z^* \sim \Delta u/Z^* \ln(l/z_0). \tag{5.6a}$$

The shear-stress perturbation in the inner region then has magnitude

$$\Delta\tau \sim u_* l \frac{\Delta u}{l\ln(l/z_0)} \sim u_* \frac{l}{L}\Delta u \sim \frac{H}{L}u_*^2. \tag{5.6b}$$

In order to estimate the height to which the mixing-length model is appropriate, the transport equation for the kinetic-energy perturbation, Δk, is analysed. In this equation, the advection of turbulent kinetic energy by the mean flow is the first term to change the equilibrium balance between production and the rate of dissipation as the height increases (see figure 6). This advection has a linearized contribution that may be written

$$U_B \frac{\partial\Delta k}{\partial X^*} = \mathrm{i}s\frac{\Delta k}{T_D}, \tag{5.7}$$

which is in phase with the slope of the undulation. The turbulent kinetic-energy equation then reduces to a balance between production, dissipation and advection, which, on using (5.5) to relate the kinetic-energy perturbation to the shear-stress perturbation, becomes

$$\Delta\tau\left[1 - 2\mathrm{i}s\frac{T_L}{T_D}\frac{k}{\overline{u'w'}}\right] = 2\kappa^2 Z \frac{U_0}{u_*}\frac{\partial\Delta u}{\partial Z}, \tag{5.8}$$

where k is the turbulent kinetic energy in the approach flow. Hence the mixing-length formula is a good approximation for the shear-stress perturbation when

$$\left|2\frac{T_L}{T_D}\frac{k}{\overline{u'w'}}\right| \ll 1. \tag{5.9}$$

Using the equilibrium-layer stress ratios, (5.5*b*), and that $T_L/T_D = 2\kappa^2(Z^*/l)(1+O(\epsilon))$, the advective effects are of the same order as the production and dissipation when

$$Z^* \sim \left|\frac{1}{4\kappa^2}\frac{\overline{u'w'}}{k}\right| l \approx \tfrac{1}{3}l, \tag{5.10}$$

i.e. the mixing-length approximation is valid through only the lower third of the inner region.

A striking feature of the terms that correct the leading-order equilibrium balance is their dependence on the anisotropy of the approach flow. In an equilibrium boundary layer the turbulence is far from isotropic, so that even if a more complex eddy-viscosity model (such as a $k-\epsilon$ model) is used, if the eddy viscosity is isotropic, it may well be no more accurate than the mixing-length model.

The curvature of the mean streamlines also plays a dynamic role in changing the Reynolds stresses at the top of the inner region. In the upper part of the inner region, the mean acceleration induced by the curvature, which is of

$$O(U_0 u_*/R) = O((H/L)\,U_0 u_*/L)$$

(where R is the radius of curvature of the streamline), of of the same order as the effects involving eddy–eddy interactions, which are $O((H/L)u_*^2/l)$ (Zeman & Jensen 1987).

Figure 7(*a*, *b*) shows comparisons of the shear-stress perturbation calculated using the linear theory and the results of Newley's (1986) calculations. In this plot $H/L = 0.04$ and $L/z_0 = 2500$. Figure 7(*a*) shows how, at the crest (where only the real part of the Fourier transform of the perturbation is non-zero), the mixing-length model is satisfactory throughout the inner region. On the upwind slope (where the imaginary part of the Fourier transform is relevant), the agreement between the mixing-length model and second-order closure is not as good. The assumption of a local equilibrium is less accurate on the slopes of a sinusoidal undulation where the advective effects (i.e. advection of turbulent kinetic energy and the 'rapid effects') are sufficiently strong that they affect the Reynolds stresses even near the surface and even at very low slopes (see figure 7*b*).

5.3. *Outer region*

In the outer region, where $Z = O(1)$ and $T_D/T_L < 1$, the 'time of flight' of an eddy is less than the eddy–eddy interaction time. The changes to the turbulence are then 'rapid' (Hunt 1978), i.e. dependent on the history of the mean flow strain and not on the local velocity gradient. The leading-order changes to the mean flow in the outer region are inviscid and the changes to the Reynolds stresses can be calculated analytically using rapid distortion theory (as demonstrated by Britter, Hunt & Richards 1981, and in §5.3.2). For example, the changes to the streamwise-velocity variance, $\Delta\overline{u'^2}$, have magnitude

$$\Delta\overline{u'^2}/\overline{u'^2} \sim \Delta u/U_B(L) \sim H/L. \tag{5.11}$$

The effect on the mean flow of these changes to the turbulence may be estimated by considering the X-momentum equation:

$$U_B\frac{\partial \Delta u}{\partial X} \sim \frac{\partial \Delta\overline{u'^2}}{\partial X} \Rightarrow U_B(L)\frac{\Delta u}{L} \sim \frac{\Delta\overline{u'^2}}{L}. \tag{5.12}$$

Hence the perturbed Reynolds stress gradients lead to mean velocity perturbations of order

$$\Delta u \sim \frac{H}{L}\frac{u_*^2}{U_B^2(L)}U_B(L) \sim \frac{H}{L}\epsilon^2 U_0. \tag{5.13}$$

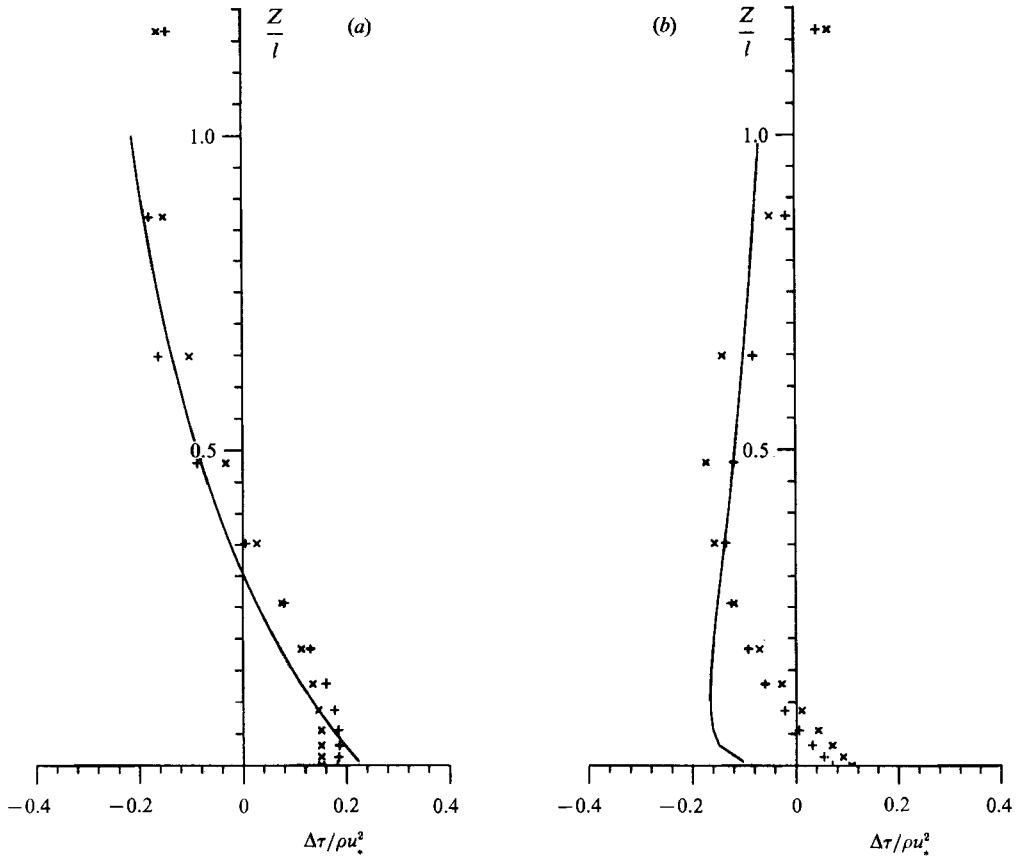

FIGURE 7. Shear-stress perturbation at (*a*) the crest, and (*b*) the upwind slope, of sinusoidal topography (with $H/L = 0.04$ and $z_0/L = 4 \times 10^{-4}$) calculated using the linear theory compared with the results computed using the second-order-closure model: ——, linear theory for the (SSL) to $O(\varepsilon^0)$; ×, $\Delta\tau/(\rho u_*^2)$ above crest in (*a*) (or upwind slope in *b*) from the second-order-closure model; +, $-\Delta\tau/(\rho u_*^2)$ above trough in (*a*) (or downwind slope in *b*) from the second-order-closure model.

The effects of the Reynolds stresses on the mean flow perturbations are thus of $O(\epsilon^2)$ in the outer region.

5.3.1. *Errors associated with eddy viscosity and mixing-length models in the outer region*

Figure 8 shows profiles of the shear stress at the summit of an isolated hill computed with the mixing-length and second-order-closure models, together with comparisons with field data. These profiles demonstrate that if the 'history effects' are accounted for through the rapid distortion mechanism, as they are in the second order closure model, the shear-stress perturbation is small and in better agreement with the experimental observations (see also Zeman & Jensen 1987). For the flow over sinusoidal topography, the shear stress perturbation in the outer region is small and positive (Newley 1986; see also Belcher & Hunt 1993*a*).

If the shear stress is approximated by an eddy-viscosity model, as in, for example, mixing-length or $k-\epsilon$ models, then the shear-stress perturbation is

$$\Delta\tau = \nu_t\left(\frac{\partial\Delta u}{\partial Z} + \frac{\partial\Delta w}{\partial X}\right), \tag{5.14}$$

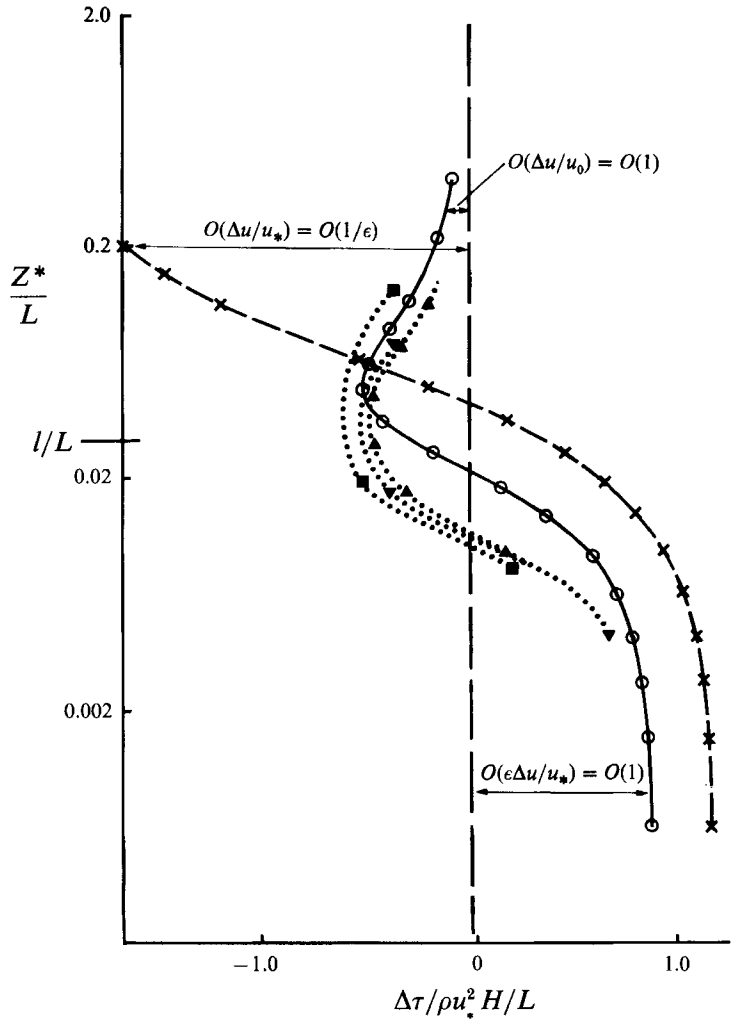

FIGURE 8. Values of the shear-stress perturbations at the crest of an isolated hill computed using the second-order-closure and mixing-length models (with the same hill shape and parameters as the numerical results in figure 4*c*), together with comparisons with field data. Note how the second-order closure model, which is in good agreement with the field data, shows a small perturbation in the outer region, whereas the mixing-length model erroneously predicts a large negative perturbation: ——, upwind profile; —O—, numerical results using the second-order-closure model; — × —, numerical results using the mixing-length model; ▲, field data for Askervein (reported in Zeman & Jensen 1987); ▼, field data for Nyland hill (Mason 1986*b*); ■, field data for Blashaval (Mason & King 1985).

for some strictly positive eddy viscosity ν_t. The gradient of the streamwise velocity perturbation is negative throughout the outer region (see figure 4*a–c*, also computed using the second-order-closure model), so that the shear-stress perturbation calculated from the eddy-viscosity model is incorrectly predicted to be negative for all topography: using the potential flow solutions, the change to the shear stress in the upper layer with the eddy-viscosity model (5.14) is

$$\Delta\tau = -\frac{2\nu_t}{L}\Delta u < 0. \tag{5.15}$$

Furthermore, if the eddy viscosity in the outer region is prescribed using the mixing-length model the predicted changes in the Reynolds stresses have the wrong sign and magnitude! The mixing-length model may be written

$$\Delta\tau \propto u_* l_m \frac{\partial \Delta u}{\partial Z^*}. \tag{5.16}$$

If the mixing length, l_m is related to the height above the surface, Z^*, which is of $O(L)$ in the upper layer, then the magnitude of the shear stress change is

$$\frac{\Delta\tau}{u_*^2} \sim \frac{U_0}{u_*}\frac{l_m}{L}\frac{\Delta u}{U_0} \sim \frac{H}{L}\frac{U(L)}{u_*}. \tag{5.17}$$

This implies a mean velocity perturbation of $O((H/L)(u_*/U_0)U_B(L))$, i.e. too large compared with (5.13) by a factor $U_B(L)/u_* = O(1/\epsilon)$. A large, negative, shear-stress perturbation is indeed observed in the values computed with the mixing-length model and plotted in figure 8.

5.3.2. *A rapid distortion model of the upper-layer turbulence distortion*

Rapid distortion theory has been used by Britter *et al.* (1981) to calculate the changes induced in an initially isotropic turbulence at the crest of a hill. We now generalize their results, first by considering the form of the distortion due to the mean flow in the whole of the perturbed region, and second by considering an initially axisymmetric turbulence (as a convenient example of anisotropic turbulence). We focus on the upper layer and then it is most convenient to perform this analysis in the Cartesian coordinates (x^*, z^*). In the upper layer the mean flow distortion is irrotational and hence may be decomposed into an irrotational strain and a rotation. The rapid effect of these two distortions on the turbulence may then be considered separately.

The specific form of the spectrum function of the initially axisymmetric turbulence is the same as used by Maxey (1982), namely

$$\Phi_{ij}(\boldsymbol{m}) = B_1\left[\delta_{ij} - \frac{m_i m_j}{m^2}\right] + B_2\left[r_i r_j + \frac{(\boldsymbol{m}\cdot\boldsymbol{r})^2}{m^2}\delta_{ij} - \frac{\boldsymbol{m}\cdot\boldsymbol{r}}{m^2}(r_i m_j + r_j m_i)\right]. \tag{5.18}$$

Here $\boldsymbol{r}$ is a unit vector along the axis of symmetry and B_1, B_2 are arbitrary functions of $|\boldsymbol{m}|$ only and which can be related to the anisotropy $S = \overline{u'^2}/\overline{v'^2} = \overline{u'^2}/\overline{w'^2}$ (Newley 1986). For a small contraction, i.e. $\Delta u/U_0 \ll 1$, the rapid distortions due to the irrotational strain are given by

$$\left.\begin{aligned}
\frac{\Delta\overline{u'^2}}{\overline{u'^2}} &= -\frac{4}{5}\frac{\Delta u}{U_0} + O\left[\left(\frac{\Delta u}{U_0}\right)^2\right],\\
\frac{\Delta\overline{v'^2}}{\overline{v'^2}} &= -\frac{4}{5}(S-1)\frac{\Delta u}{U_0} + O\left[\left(\frac{\Delta u}{U_0}\right)^2\right],\\
\frac{\Delta\overline{w'^2}}{\overline{w'^2}} &= (\tfrac{6}{5} - \tfrac{2}{5}S)\frac{\Delta u}{U_0} + O\left[\left(\frac{\Delta u}{U_0}\right)^2\right].
\end{aligned}\right\} \tag{5.19}$$

(Full details of this calculation may be found in Newley 1986). The trends and signs of the effects of anisotropy agree with analytical solutions obtained in the 'rapid limit' of the second-order-closure model of LRR and that used by Zeman & Jensen (1987), but the numerical coefficients differ slightly. This idealized calculation shows that the second-order closure models should give the correct order of magnitude for the normal stress changes induced in the outer region.

Comparisons of the formulae (5.19) at the crest of an isolated hill with the results computed using the second-order-closure model are presented in figure 9. Note how the second-order-model computations for $\overline{w'^2}$ are closer to the RDT results of (5.19) obtained using anisotropic, rather than isotropic, upstream turbulence. The experimental evidence (see Zeman & Jensen 1987, and Mason & King 1985) suggests that, in contrast to the second-order-closure model results, $\overline{w'^2}$ increases slightly in the outer region (it is likely that the second-order-closure models overestimate the 'return to isotropy' for rapidly changing flows).

The rapid distortion calculations presented by Townsend (1980) show that, at leading order in H/L, the rotation by the curvature of the mean streamlines has only a kinematic effect on the Reynolds stresses, i.e. the changes may be obtained by rotating the stress tensor into the displaced coordinate system (see (2.7)). This agrees with the suggestion of Zeman & Jensen (1987) that the curvature effects on the turbulence stresses are of $O(H^2/L^2)$ in the upper layer at the crest of the undulation.

The overall changes to the Cartesian components of the stress are then formed by adding the two perturbations, (5.19) and (2.7).

5.4. *Discussion*

These scaling arguments, together with the analysis of the numerical results, suggest definite criteria that any turbulence model must satisfy if it is to predict correctly the perturbations to the Reynolds stresses in any turbulent boundary layer that is subjected to a rapidly varying pressure gradient (rapid in the sense that $L \ll hU_B(L)/u_*$). It is crucial to consider separately the turbulence in the approach flow and the turbulence changes induced by the pressure gradient: many authors have erroneously assumed that, because a mixing-length model can satisfactorily be used to calculate a fully developed boundary layer that is changing slowly, it can also be used to model the perturbations to a turbulent boundary layer changing on a lengthscale less than $h_*(= hU(L)/u_*)$.

Firstly, the height l above the surface marks a change in character of the response of the turbulence to the perturbation. Any turbulence model that is general enough to describe fully a range of perturbed boundary layers must be valid above and below this transition height.

Secondly, at heights $Z = O(1)$ the perturbations to the turbulence are largely governed by the rapid distortion mechanism. The quantitative changes to the Reynolds stresses are dependent on the anisotropy of the turbulence in the approach flow (as shown by the calculation of the rapid contraction of axisymmetric turbulence, equation (5.19)). Hence if the approach flow turbulence is not well specified it is not possible to calculate accurately the changes induced by the perturbation. Any turbulence model for the outer region that is based on an eddy-viscosity hypothesis gives perturbations to the shear stress of the wrong sign. Furthermore, the mixing-length model implies shear stress perturbations in the outer region that are a factor of $O(1/\epsilon)$ too large – this leads to 'integrated' properties (e.g. the net drag change on the surface) also being $O(1/\epsilon)$ too large (see §8 below).

Thirdly, in the lower third of the inner region the perturbations to the turbulence are close to local equilibrium and a mixing-length model is appropriate. In the upper two thirds of the inner region the advection of perturbed turbulent kinetic energy by the mean flow is of the same order as the rates of production and dissipation. This effect is greatest at the sloping parts of a hill, where the large accelerations in the mean flow occur. The corrections to the mixing-length formula are also dependent on the anisotropy of the approach flow, so an isotropic eddy-viscosity model cannot predict

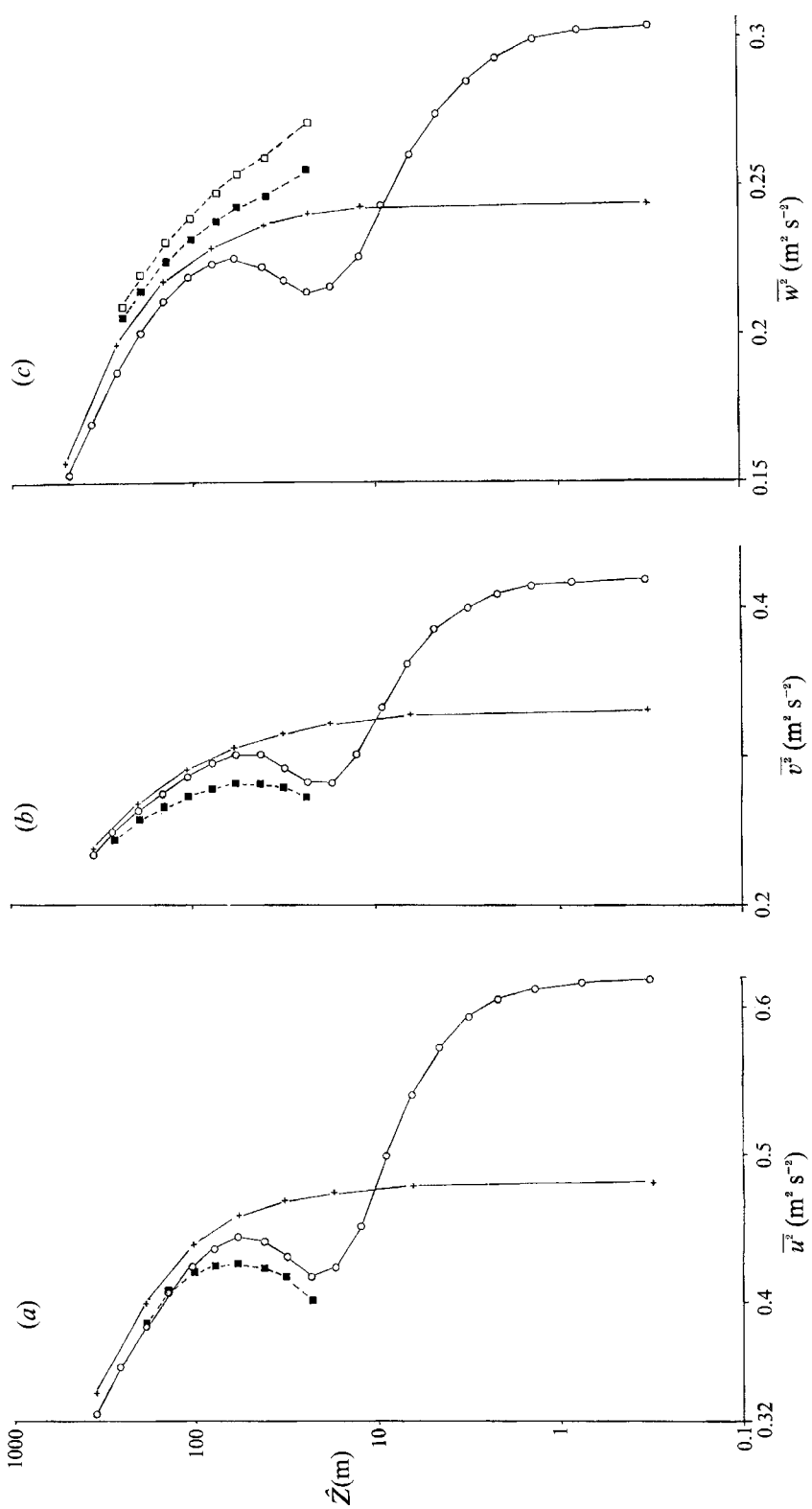

FIGURE 9. The perturbations to the turbulence variances at the crest of an isolated hill (with the same parameters as the numerical results in figure 4*c*) calculated using rapid distortion theory (using the computed values of the velocity perturbation) and compared with the results of the second-order-closure model. (*a*) $\overline{u^2}$; (*b*) $\overline{v^2}$; (*c*) $\overline{w^2}$. —+—, Upwind values; – – –■– – –, axisymmetric RDT with $R = 2$; – – –□– – –, isotropic RDT; —○—, results from LRR closure model.

reliably these aspects of the flow perturbations. However, the effects of the accelerations integrated over their streamwise extent determine the maximum shear stress and peak velocity at the summit of the hill and these values are adequately modelled by using the mixing-length model throughout the inner region (see also Tampieri 1987). Since the drag on the surface is an integrated effect, it is reasonable to expect that calculations using the linear model should be in fair agreement with those obtained using the LRR turbulence model and with experiments (see §8).

6. Estimates of the asymmetric pressure from other effects

We now return to the analytic model and determine the magnitudes of the corrections to the non-separated sheltering contribution to the asymmetric pressure perturbation. This is done by examining how asymmetric pressure perturbations are generated in (2.28*a*) by the other physical mechanisms that were discussed in the introduction. Particular care must be exercised in estimating the effects of the Reynolds stresses on the pressure perturbation because of the two-layer structure of the turbulence perturbation. Hence we consider separately the inner and outer regions.

6.1. *Inner-region Reynolds-stress effects*

The effect of the perturbed Reynolds stresses on the out-of-phase pressure perturbation within the inner region is now examined. Only effects within the shear-stress layer are considered: the (ISL) is so thin that the variation in the pressure across it is exponentially small (i.e. $O(\mathrm{e}^{-1/\epsilon})$).

Rewriting (2.28*a*) using inner-region variables, the equation governing how the pressure reacts to the Reynolds stress perturbations in the inner region is

$$\frac{\partial^2 p_{\mathrm{d}}^{(\mathrm{IRS})}}{\partial \zeta^2} = -\epsilon^2\left[-4\kappa^2 s^2 \frac{\epsilon^2}{U^2(l)}\tau_{XX} + \frac{\partial^2 \tau_{ZZ}}{\partial \zeta^2} + 2\mathrm{i}s\frac{2\kappa\epsilon}{U(l)}\frac{\partial \tau_{\mathrm{d}}}{\partial \zeta}\right]. \tag{6.1}$$

The effect of the Reynolds stresses on the surface pressure variation in the inner region is thus of second order in ϵ and is given by

$$p_{\mathrm{d}}^{(\mathrm{IRS})}(s,\zeta) = -\epsilon^2\left[\tau_{ZZ}(s,\zeta) - 2\mathrm{i}s2\kappa\frac{\epsilon}{U(l)}\int_{\zeta}^{\infty}\tau_{\mathrm{d}}\,\mathrm{d}\zeta' + 4\kappa^2 s^2\frac{\epsilon^2}{U^2(l)}\int_{\zeta}^{\infty}\int_{\zeta'}^{\infty}\tau_{XX}\,\mathrm{d}\zeta''\,\mathrm{d}\zeta'\right]. \tag{6.2}$$

The different components of the Reynolds stress affect the pressure in fundamentally different ways: it is the *local* value of τ_{ZZ} which causes the pressure change; whereas, τ_{d} and τ_{XX} both have *non-local* effects since their contribution to the solution (6.2) are integrated. Hence to calculate the surface pressure requires that τ_{ZZ} be modelled correctly only near the surface, but the other two terms must be correctly modelled throughout the inner region.

The normal stresses are modelled according to (5.5). The surface stress has an out-of-phase component of $O((H/L)u_*^2\,\epsilon)$ (see HLR, and the Appendix) so that τ_{ZZ} leads to an asymmetric pressure perturbation of $O(\rho U_0^2\,\epsilon^3)$. The integral over the shear stress in (6.2) also leads to an $O(\rho U_0^2\,\epsilon^3)$ asymmetric pressure perturbation. Hence the inner-region Reynolds-stress effects lead to a correction to the asymmetric surface pressure that is $O(\epsilon)$ smaller than the contribution from non-separated sheltering (see §3).

6.2. *Outer-region Reynolds-stress effects*

Throughout the outer region the leading-order changes to the Reynolds stresses are determined by the rapid distortion mechanism. In order to estimate the effect on the

out-of-phase pressure, we focus on the upper layer. The magnitudes of the changes to the stresses are also the same in the middle layer, but the $O(1)$ coefficients from the rapid distortion calculation are different because of the significance of the mean shear in the approach flow through the middle layer.

In the upper layer the mean-flow distortion of the turbulence is composed of two parts: a rotation and an irrotational strain. The effect of the rotation is discussed in §6.3 below, here only the irrotational strain is considered.

The relevant terms of (2.28*a*) are

$$\frac{\partial^2 p_{\mathrm{d}}^{(\mathrm{ORS})}}{\partial Z^2} - s^2 p_{\mathrm{d}}^{(\mathrm{ORS})} = -\epsilon^2 \left[-s^2 \tau_{XX} + \frac{\partial^2 \tau_{ZZ}}{\partial Z^2} + 2\mathrm{i}s \frac{\partial \tau_{\mathrm{d}}}{\partial Z} \right]. \tag{6.3}$$

As explained in §5.3.2, rapid distortion theory shows that the changes to the stress components may be expanded as power series in the velocity perturbation:

$$\frac{\Delta \tau_{XX}}{\tau_{XX}} = A \frac{\Delta u}{U_0} + O\left(\frac{H^2}{L^2}\right), \tag{6.4}$$

where A is the $O(1)$ constant from rapid distortion theory.

The velocity perturbation is inviscid and irrotational and so using (6.4) the linear forcing term on the right-hand side of (6.3) is a linear combination of $\tilde{G}$ and $\tilde{G}'$. The particular solution for the pressure is then a linear combination of $sZ\tilde{G}$ and $sZ\tilde{G}'$. These terms are negligibly small ($O(z_0/L)$) at the surface and hence cannot affect the drag directly; they can, however, augment the non-separated sheltering, via an indirect mechanism.

To complete the solution for the linear part of $p_{\mathrm{d}}^{(\mathrm{ORS})}$, a multiple of the appropriate solution to the homogeneous equation is also required. This arises from the balances between the pressure and stress gradients in the X- and Z-momentum equations, namely

$$\frac{\partial p_{\mathrm{d}}}{\partial X} \sim \epsilon^2 \frac{\partial \tau_{XX}}{\partial X}, \quad \frac{\partial p_{\mathrm{d}}}{\partial Z} \sim \epsilon^2 \frac{\partial \tau_{ZZ}}{\partial Z}. \tag{6.5}$$

Equations (6.4) and (6.5) then imply that the homogeneous solution is proportional to $\epsilon^2 \Delta u / U_0$. The non-separated sheltering leads to an asymmetric velocity perturbation of $O((H/L)\, U_0 \epsilon^2)$ in the outer region (see §3) and thence, through the homogeneous solution, to an asymmetric pressure perturbation of $O(\rho U_0^2 (H/L) \epsilon^4)$, which is of $O(\epsilon^2)$ smaller than the direct effect of non-separated sheltering.

These arguments may be extended to consider the $O(H^2/L^2)$ pressure perturbations that are induced in the outer region. At $O(H^2/L^2)$ the velocity perturbation has components that are proportional to $\mathrm{e}^{-2sZ/L}$ which lead to a pressure perturbation that has a significant value at the surface. This velocity perturbation leads, via (6.4), to Reynolds-stress perturbations of $O((H^2/L^2) u_*^2)$. This leads to an asymmetric pressure perturbation of $O(\rho U_0^2 (H^2/L^2) \epsilon^2)$.

Hence we estimate that the direct effects of the outer-region Reynolds-stress perturbations on the asymmetric surface pressure are of order

$$\mathrm{Asym}\,[p_{\mathrm{d}}^{(\mathrm{ORS})}] = O\left(\rho U_0^2 \frac{H}{L} \epsilon^4, \rho U_0^2 \frac{H^2}{L^2} \epsilon^2 \right). \tag{6.6}$$

The rapid distortion of the turbulence in the outer region also has an effect on the asymmetric pressure perturbation through an indirect mechanism. The particular solution to (6.3) is in phase with the topography and equal to

$$p_{\mathrm{d}}^{(\mathrm{ORS})} = \epsilon^2 A s Z f \tilde{G}' = 2(\epsilon^3/\kappa) A \hat{\sigma}^{(0)} \zeta, \tag{6.7}$$

where A is the $O(1)$ coefficient from rapid distortion theory. This pressure perturbation further accelerates the inner-region flow, since it provides a forcing for the equation governing the streamwise velocity perturbations in the (SSL), namely

$$\frac{\partial}{\partial\zeta}\left(\zeta\frac{\partial u_{\mathrm{d}}^{(\mathrm{ORS})}}{\partial\zeta}\right)-\mathrm{i}su_{\mathrm{d}}^{(\mathrm{ORS})}=-\mathrm{i}sp_{\mathrm{d}}^{(\mathrm{ORS})}. \tag{6.8}$$

The particular solution for the streamwise velocity perturbation is then

$$u_{\mathrm{d}}^{(\mathrm{ORS})}=2U(l)\,(\epsilon^3/\kappa)\,A(s\zeta-\mathrm{i})\,\hat{\sigma}^{(0)}. \tag{6.9}$$

The first part of this solution is in phase with the topography and is just the inviscid acceleration of the mean flow by the pressure perturbation; the second part, proportional to $\mathrm{i}\hat{\sigma}^{(0)}$, is out of phase with the undulation and is due to the interaction between the linearly varying $p_{\mathrm{d}}^{(\mathrm{ORS})}$ and the shear-stress gradient. Furthermore, this second part of the velocity perturbation is constant so that it is non-zero at the top of the inner region, thereby adding to the non-separated sheltering effect. The out-of-phase pressure perturbation which develops in the outer region is

$$\mathrm{Asym}\,[p_{\mathrm{d}}]=\rho U_0^2\frac{H}{L}2U(l)\frac{\epsilon^3}{\kappa}A\mathrm{i}s\tilde{f}\tilde{G}'=O\left(\rho U_0^2\frac{H}{L}\epsilon^3\right), \tag{6.10}$$

which is $O(\epsilon)$ smaller than the non-separated sheltering effect calculated in §3. This process is a result of a balance, at the height of $O(l)$, between the limiting behaviour of the two turbulence perturbations (namely the rapid and equilibrium mechanisms), hence we recognize that the present model may not give an accurate numerical value of this effect (mainly because the mixing-length model is not adequate at the top of the inner region, §5).

6.3. *Effects of mean streamline curvature*

Equation (2.28*a*) is expressed in the displaced coordinate system and hence contains the linear effects of mean streamline curvature. The curvature-induced pressure perturbation is then governed by

$$\frac{\partial^2 p_{\mathrm{d}}^{(\mathrm{SC})}}{\partial Z^2}-s^2p_{\mathrm{d}}^{(\mathrm{SC})}=-\tilde{f}\tilde{G}\left[2U'Us^2-\epsilon^2\left(4\mathrm{i}s^3+2s^3(T_{XX}-T_{ZZ})\right)\right]. \tag{6.11}$$

The first term on the right-hand side leads to the inviscid rotational pressure perturbation caused by the coordinate transformation and hence cannot induce any out-of-phase perturbations. The second set of terms on the right-hand side of (6.11) arises from the transformation of the Reynolds-stress tensor into the displaced coordinate system, and are equivalent to the linear part of the rapid distortion caused by the streamline curvature (§5.3.2). Hence the only linear effect of rotation that provides an asymmetric pressure perturbation is the deformation of the normal Reynolds stresses, i.e. the last terms in (6.11).

These terms have the same mathematical form as the forcings induced by the rapid contraction of the turbulence, which are discussed in §6.2 above. Hence the asymmetric pressure induced by the curvature has components of $O((H/L)\epsilon^4, (H^2/L^2)\epsilon^2)$ from the direct mechanisms. The curvature also augments the non-separated sheltering, leading to an asymmetric pressure of $O(\rho(H/L)\,U_0^2\,\epsilon^3)$.

7. The pressure force on arbitrary terrain

The zeroth-order surface pressure coefficient over arbitrary terrain can be evaluated from its Fourier transform (see Appendix (A 5)) using the convolution theorem and is

$$\sigma^{(0)}(X) = \frac{1}{\pi}\int_{-\infty}^{\infty} \frac{f'(y)}{X-y}\mathrm{d}y. \tag{7.1}$$

Using this expression, we find that its contribution to the drag force is

$$\Delta F^{(p^{(0)})} \propto \int_{-\infty}^{\infty}\int_{-\infty}^{\infty} \frac{f'(x)f'(y)}{x-y}\mathrm{d}x\,\mathrm{d}y, \tag{7.2}$$

which is antisymmetric in x and y and hence zero. This result is just a consequence of the $O(\epsilon^0)$ pressure perturbation being determined by inviscid dynamics. The contribution from the real part of the $O(\epsilon)$ and $O(\epsilon^2)$ pressure perturbations are also zero: this is explained as follows. These pressure terms must be linear in $\sigma^{(0)}$, and proportional to some integral power of the wavenumber, s. The higher the power of s in the real part of the second-order pressure, the higher the derivative of f in the convolution integral for the pressure in physical space. Integrating by parts shows that the resulting contribution to the drag is zero for any power of s. Hence the leading-order drag perturbation is entirely due to the out-of-phase component of the pressure perturbation.

We have shown that the leading-order contribution to the out-of-phase pressure perturbation arises from the non-separated sheltering effect. The analysis of HLR has been extended to show that the Fourier transform of the asymmetric pressure induced by the non-separated sheltering is

$$\mathrm{Im}\,[p_{\mathrm{d}}^{(\mathrm{NSS})}] = -\frac{4\epsilon^2}{U^4(l)}\mathrm{i}\sigma^{(0)}, \tag{7.3}$$

where $\sigma^{(0)} = s\tilde{f}\tilde{G}'(0)$. Using the convolution theorem the Fourier transform may be inverted and the asymmetric pressure expressed as

$$\mathrm{Asym}\,[p_{\mathrm{d}}^{(\mathrm{NSS})}(x,z_0)] = -\frac{4\epsilon^2}{U^4(l)}\frac{1}{2\pi}\int_{-\infty}^{\infty} f'(y)\,G'(x-y,0)\,\mathrm{d}y, \tag{7.4}$$

where $G'(x,Z)$ is the inverse Fourier transform of $\tilde{G}'$. The leading-order pressure force is then given by

$$\Delta F_p = -\frac{H^2}{L^2}L\rho u_*^2\left[\frac{4}{U^4(l)}\frac{1}{2\pi}\int\!\!\int_{-\infty}^{\infty} f'(x)f'(y)\,G'(x-y,0)\,\mathrm{d}x\,\mathrm{d}y + O(\epsilon)\right]. \tag{7.5}$$

Then for neutral flow that is unbounded in the vertical, $\tilde{G}'(s,0) = -1$ and the aerodynamic drag becomes

$$\Delta F_p = \frac{H^2}{L^2}L\rho u_*^2\left[\frac{4}{U^4(l)} + O(\epsilon)\right]\int_{-\infty}^{\infty} f'^2(x)\,\mathrm{d}x. \tag{7.6}$$

This expression for the perturbation pressure force scales on the square of u_*, the approach flow friction velocity, which is determined by the Reynolds number of the flow for aerodynamically smooth surfaces or by z_0, the roughness length, when the surface is rough. Furthermore, the expression varies with $U(l) = U_{\mathrm{B}}(l)/U_{\mathrm{B}}(h_{\mathrm{m}})$, the shear in the upwind velocity profile across the middle layer. This parameter also varies

with the Reynolds number, or relative roughness length, since it is dependent on $u_*/U_0 = O(\ln^{-1}(L/z_0))$. For example, when the lengthscale of the hill is sufficiently short that the approach flow profile is logarithmic through the middle layer,

$$U(l) \sim 1 + O(\epsilon \ln(1/\epsilon)) \quad \text{as} \quad \epsilon \to 0. \tag{7.7}$$

This variation of the drag with ϵ is important for practical purposes.

8. Comparison with other studies

When the topography is sinusoidal, (7.6) shows that the drag force is given by

$$\Delta F_p = \frac{H^2}{L^2} \rho u_*^2 L \left[\frac{4}{U^4(l)} + O(\epsilon) \right] \tfrac{1}{2}\pi^2. \tag{8.1}$$

Figure 10 shows the variation of the perturbation pressure force with slope, H/L, for sinusoidal terrain. The analytical result (8.1), which predicts quadratic dependence, is compared with the experimental values obtained by Zilker & Hanratty (1979) and the values computed using the second-order-closure and mixing-length models. The theoretical curve is plotted for $\ln^{-1}(L/z_0) = 0.1$. The normalization used for ΔF is such that a value of one corresponds to a perturbation drag force that is equal to the drag on an equivalent length of flat terrain. The graph shows that the linear theory is in excellent agreement up to $\pi H/2L \approx 0.3$, i.e. up to $H/L \approx 0.2$. Even at these low slopes the terrain induces a perturbation drag that is half to three-quarters as large as the unperturbed value. For slightly higher slopes, according to the calculations performed with the second-order-closure model, the drag increases approximately linearly, and can be double the value of the unperturbed drag (so that the total drag is three times the value for level terrain). For $\pi H/2L$ larger than about 0.5 (i.e. H/L greater than about 0.3) the increase in the drag flattens, indicating that the mean flow has separated (field measurements confirm this estimate for the slope required to induce separation).

The values in figure 10 for the drag obtained numerically using the mixing-length model are consistently larger than those from the theory and the values obtained numerically using the second-order-closure model. In the domain of validity of the linear theory, the mixing length predicts values of the perturbation drag that are about 100% larger than the theory, experiments and second-order-closure model results (see the discussion of figure 11). At the larger slopes the relative difference is smaller but still significant (about 17% for $H/L = 0.3$). The experimental data show similar trends to the results obtained with the models, but are too sparse to enable a quantitative comparison to be made over the whole range of slopes between the performances of the theory, and the mixing-length and second-order-closure models – a more complete set of experimental measurements would certainly be useful.

We now focus on low slopes and make a more detailed comparison between the various methods. Figure 11 shows the variation of the drag coefficient, $\Delta F_p/(H^2/L^2)\rho u_*^2 L$, for sinusoidal topography, with the parameter $\ln^{-1}(L/z_0) = O(\epsilon)$, which is of the order of $\ln^{-1}(Re_L)$ for smooth surfaces (the Reynolds number is defined as $Re_L = u_* L/\nu$). The theoretical result (8.1) is compared with the values obtained from the experiments of Zilker & Hanratty (1979), Townsend's (1972, 1980) computations together with the present computations. The results are for the pressure force only, i.e. the contribution from the $O(H^2/L^2)$ shear-stress perturbation is not included. In figure 11 the slope of the undulation, H/L, ranges from 0.04 to 0.16 (hence the scatter in the computed data is due to nonlinear effects).

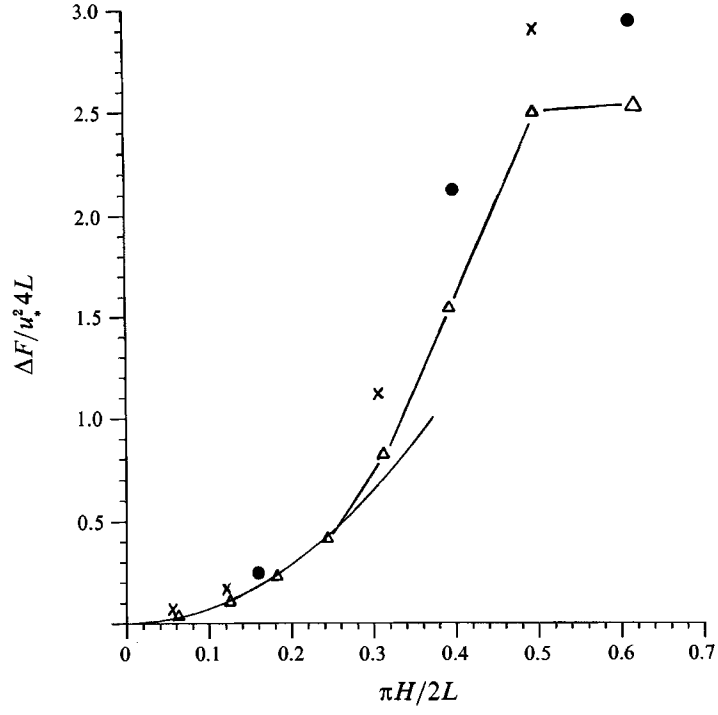

FIGURE 10. Variation of the perturbation drag force with slope for sinusoidal topography: ——, linear theory (with $\ln^{-1} L/z_0 = 0.1$); ●, experimental results of Zilker & Hanratty (1979); ×, results computed using the mixing-length model; —△—, results computed using the second-order-closure model.

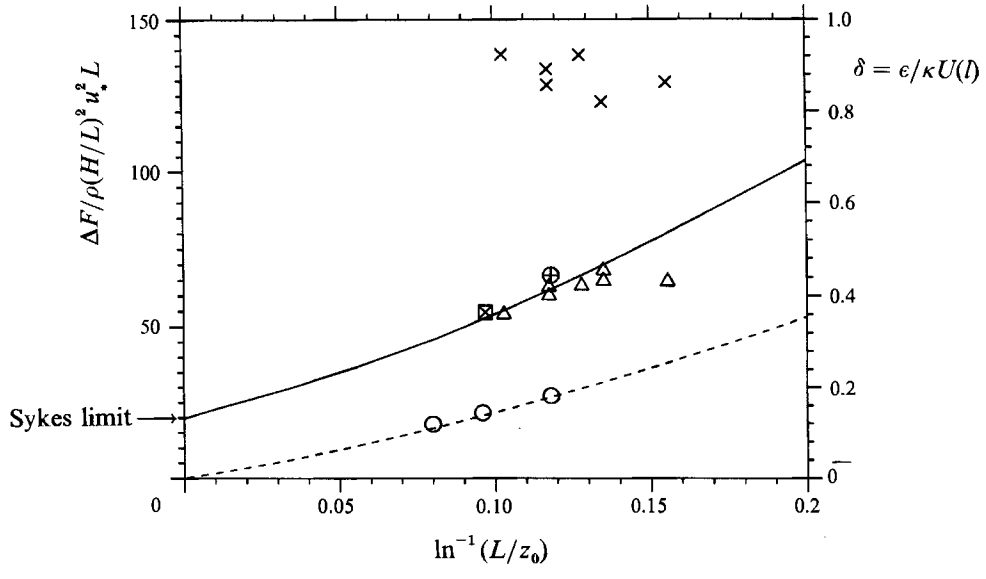

FIGURE 11. Variation of the perturbation drag coefficient with relative surface roughness for sinusoidal terrain: – – –, variation of $\delta = \epsilon/\kappa U(l)$ (right scale); ——, drag coefficient from linear theory (left scale); △, drag coefficient computed using the second-order-closure model; ×, drag coefficient computed using the mixing-length model; ○, drag coefficient computed by Townsend (1972); ⊕, drag coefficient computed by Townsend (1980); ⊠, drag coefficient from experimental results of Zilker & Hanratty (1979).

The formula for the leading-order drag coefficient, which is due to the non-separated sheltering, is within about 10% of the results of experiments and those obtained using the second-order turbulence closure model. (The rightmost value computed using the second-order-closure model is for the largest value of the slope, $H/L = 0.16$, and is furthest from the linear model.) As explained in §3.1, the good agreement follows from the good quantitative agreement between the shear-stress perturbation at the crest of the undulation predicted by the theory and the results of numerical calculations with the second-order closure.

The results computed with the second-order-closure model are, of course, only approximate: in particular, the anisotropy of the turbulence in the approach flow is not modelled correctly (§4.2). The theoretical model shows that at leading order the non-separated sheltering is unaffected by the anisotropy of the approach flow; the further analysis of §6 suggests, however, that the (assumed) anisotropy of the approach flow changes the coefficients (but not the magnitudes) of all the $O(\epsilon)$ corrections to the non-separated sheltering value of the drag.

The results obtained numerically using the mixing-length formula throughout the flow are more than 100% larger than both the theoretical curve and the results using the second-order closure model. The reason is that estimating the shear-stress perturbation with the mixing-length model implies a balance, in the outer region, between the inertial and shear-stress gradients at $O(\epsilon)$ (correctly using rapid distortion theory in the outer region implies that this balance occurs at $O(\epsilon^2)$, see §5.3.1). Hence using mixing length in the outer region leads to an out-of-phase pressure perturbation of $O(\rho U_0^2 \epsilon)$, and thence the perturbation drag force is too large by a factor of $1/\epsilon$. This is confirmed by the detailed calculation of Jacobs (1987), who has calculated the asymmetric pressure perturbation using a mixing-length model throughout the flow and thereby attributed the leading-order drag force to outer-region Reynolds stress effects. We have argued that this conclusion is not correct, since it is based on an inappropriate use of the mixing-length model.

Sykes (1980) has calculated, as asymptotic sequences in the limit $\epsilon = u_*/U_0 \to 0$, the perturbations to a turbulent boundary layer passing over a wall-mounted obstacle. In his study, the slope of the hump is scaled on the dimensionless friction velocity, so that $H/L = \epsilon^{\frac{1}{2}}$, and hence Sykes' analysis is valid for only asymptotically small undulations. Using the asymptotic solutions, Sykes calculated the pressure drag force and found

$$\Delta F_p = 4\rho u_*^2 L\epsilon \int f'^2 \,\mathrm{d}x \quad \text{as} \quad \epsilon \to 0. \tag{8.2}$$

Sykes then inferred that, since his expression for the perturbation drag is proportional to ϵ, the drag is proportional to H^2/L^2.

From (7.7), in the limit of $\epsilon \to 0$, $U(l) \to 1$ and there is no shear in the approach flow through the depth of the middle layer. The result of the present analysis, (7.6), hence agrees with (8.2) in the limit $\epsilon \to 0$, i.e. infinite Reynolds number (for smooth surfaces) or in the limit vanishing roughness length, $\ln^{-1}(L/z_0) \to 0$ (for rough surfaces). The present theory enables Sykes' result to be extended. For finite, but still small, values of ϵ, $U(l)$ can be significantly different from 1, through the $\epsilon \ln(1/\epsilon)$ correction. The variation of the drag force from its value in the Sykes limit is then large since ΔF_p depends on the fourth power of $U(l)$ and its inclusion in the analysis renders the asymptotic solution of practical value. For Sykes theory to be valid within 10% figure 11 shows that it is necessary that $\ln^{-1}(L/z_0) < 0.025$. Although the Sykes result agrees with our formula in the limit $\epsilon \to 0$, he did not explain that the leading-order drag is caused by the non-separated sheltering effect. Furthermore, our result, (8.1), is valid

for a wide class of monotonic velocity profiles in the middle layer. Stratification can significantly alter the shear across the middle layer and hence the drag. (We are currently studying this problem.)

Also plotted on figure 11 are some values inferred from the results of Townsend (1972, 1980). These numerical calculations were performed to assess the growth rate of water waves by the wind (discussed in a companion paper by Belcher & Hunt 1993*a*). In the first study, Townsend (1972) assumed that throughout the flow the changes to the Reynolds stresses are a fixed proportion of the change in turbulent kinetic energy; whereas in the present study this assumption is made only close to the surface, where it is justifiable. The turbulent kinetic energy was then solved as part of the numerical problem in order to calculate the Reynolds stresses. This calculation was extended by Townsend (1980) to account for the variation of the stress ratios due to the rapid distortion mechanism. The changes to the stress were prescribed by equations of the form

$$\frac{\Delta\overline{u'^2}}{\overline{u'^2}} = \frac{\Delta k}{k} + \frac{\Delta\alpha}{\alpha}, \tag{8.3}$$

where α is the ratio $\overline{u'^2}/k$ in an equilibrium boundary layer. Each of the stress ratios is specified by an equation of the form

$$U\frac{\partial\Delta\alpha}{\partial x} + \frac{\Delta\alpha - \alpha}{T_L} = A\frac{\partial u}{\partial x} + B\frac{\partial w}{\partial x} + C\frac{\partial u}{\partial Z}, \tag{8.4}$$

where A, B and C are determined from rapid distortion theory. This model equation implies that close to the surface the changes to the turbulence are governed largely by equilibrium dynamics, and high above the surface the changes are nearly rapid. The two effects are of the same order at the height l above the surface, i.e. at the top of the inner region. Calculations show that by including these rapid effects the value of the drag coefficient is doubled compared with the values obtained with Townsend's earlier model. The 1972 model underestimates the drag mainly because the shear-stress perturbation at the top of the inner region is too small using this turbulence model (cf. the discussion of §3.1). Townsend's (1980) method of modelling the changes to the turbulent stresses is similar to the approach adopted here and indeed the two theories are in close agreement.

9. Discussion

The present study has two main aspects. Firstly, we have derived constraints which must be satisfied by the closure model for the Reynolds stresses in order to model correctly the changes to a turbulent boundary layer that is subjected to a rapidly varying pressure gradient (i.e. $L \ll hU_B(L)/u_*$). The implications of this analysis have been described in §5.4. Secondly, we have examined the process that control how a turbulent boundary layer increases the drag force on an undulating surface.

The leading-order contribution to the drag arises from the non-separated sheltering effect, i.e. the thickening of the inner region on the leeside of the crest and the resulting asymmetry in the outer-region flow. An analytic formula has been derived for the drag induced by the non-separated sheltering by extending the analysis of Hunt, Leibovich & Richards (1988). Furthermore, estimates have been obtained for the magnitude of the contributions to the drag from the other mechanisms that are described in §1.1. These are all smaller than the non-separated sheltering effect when both H/L and ϵ are small. The orders of magnitude of the contributions to the dimensionless drag coefficient from each of the processes are summarized in table 1.

	Δp	$\Delta\tau_{xx}$	$\Delta\tau$‡
NSS	$\frac{H^2}{L_2}\epsilon^2, \frac{H^2}{L^2}\epsilon^3$†	—	—
IRS	$\frac{H^2}{L^2}\epsilon^3$	$\frac{H^2}{L^2}\epsilon^3$	NC
ORS	$\frac{H^2}{L^2}\epsilon^4$	$\frac{H^2}{L^2}\epsilon^4$	NC
FAD	$\frac{H^3}{L^3}\epsilon^2$	$\frac{H^3}{L^3}\epsilon^2$	NC

† The contributions to the drag from the second-order shear-stress perturbation have not been calculated, but the numerical results suggest that they are small (see also Sykes 1980).

‡ This correction is from the enhancement of the NSS by the ORS effects (§6.2). NC means not calculated.

TABLE 1. Orders of magnitude of the contributions to the drag (normalized on ρU_0^2) from the various mechanisms:

$$\Delta F = \int \Delta\tau \, \mathrm{d}x + \int (\Delta p - \Delta\tau_{xx}) f'(x/L) \, \mathrm{d}x$$

We have shown that at the crest of the undulation the shear-stress perturbation from the linear theory is in good agreement with the values computed using the numerical model with a second-order-closure model. The numerical magnitude of the non-separated sheltering effect is related to the component of the inner-region Reynolds-stress perturbation that is in phase with the undulation; this component of the shear-stress perturbation is adequately modelled using the mixing-length model in the inner region. The formula for the drag coefficient has been shown to agree well with numerical studies and experimental values for slopes up to about $\frac{1}{3}$, when mean flow separation occurs. Finally, including the effects of the shear across the middle layer (through the $U(l)$ term) increases the drag from the value predicted by Sykes' (1980) formula and enables the asymptotic theory to be used for practical purposes.

S. E. B. is grateful for the financial support of the SERC under a CASE studentship with AERE, Harwell. T. M. J. N. acknowledges the support of the NERC and the generous assistance of Paul Mason at the UK Met. Office, where the computations were performed. During the course of this research we benefitted from useful conversations with Alan Townsend, Otto Zeman and Wensong Weng. The suggestions of the anonymous referees are also gratefully acknowledged.

Appendix. Asymptotic solutions from HLR

The solutions are expressed in terms of the displaced coordinates, which are related to the Cartesian coordinates by

$$x = X - (H/L)\,\mathrm{i}s\tilde{f}\tilde{F}(sZ), \qquad z = Z + (H/L)\tilde{f}\tilde{G}(sZ). \tag{A 1}$$

Mean flow quantities are made non-dimensional using $U_0 = U_{\mathrm{B}}(h_{\mathrm{m}})$ and the Reynolds-stress components on ρu_*^2. The linear perturbations in the Cartesian coordinates are related to those in the displaced coordinates by

$$\left.\begin{aligned} u(z) = u_{\mathrm{d}}(Z), \quad w(z) = \mathrm{i}s\tilde{f}\tilde{G} + w_{\mathrm{d}}(Z), \quad p(z) = p_{\mathrm{d}}(Z) \\ \tau_{xx}(z) = \tau_{XX} - 2\mathrm{i}s\tilde{f}\tilde{G}, \quad \tau_{zz}(z) = \tau_{ZZ} + 2\mathrm{i}s\tilde{f}\tilde{G}, \quad \tau(z) = \tau_{\mathrm{d}} + \mathrm{i}s\tilde{f}\tilde{G}(T_{XX} - T_{ZZ})/\rho u_*^2. \end{aligned}\right\} \tag{A 2}$$

The following expressions are the solutions for the perturbations in the displaced coordinates.

A.1. *Inner-surface layer*

The vertical coordinate scales on the roughness length, z_0, and is $\eta = Z^*/z_0 = Z/((1/\epsilon)\mathrm{e}^{-\frac{1}{\epsilon}})$.

$$\left.\begin{aligned} u_{\mathrm{d}} &\sim -\frac{1}{U(l)}\left[\left\{\frac{\epsilon}{\kappa U(l)}\hat{\tau}^{(0)}(z_0)+\left(\frac{\epsilon}{\kappa U(l)}\right)^2\hat{\tau}^{(1)}+O(\epsilon^3)\right\}\ln\eta+O\left(\frac{z_0}{L}\right)\right],\\ w_{\mathrm{d}} &\sim -\frac{1}{U(l)}\left[O\left(\frac{z_0}{L}\right)\right],\\ \tau_{\mathrm{d}} &\sim -\frac{2}{U^2(l)}\left[\hat{\tau}^{(0)}+\frac{\epsilon}{\kappa U(l)}\hat{\tau}^{(1)}(z_0)+\left(\frac{\epsilon}{\kappa U(l)}\right)^2\hat{\tau}^{(2)}(z_0)+O\left(\epsilon^3,\frac{z_0}{L}\right)\right],\\ p_{\mathrm{d}} &\sim \left[\hat{\sigma}^{(0)}+O\left(\epsilon^2,\frac{z_0}{L}\right)\right], \end{aligned}\right\} \tag{A 3}$$

with
$$\hat{\tau}^{(0)} = \hat{\sigma}^{(0)}, \quad \hat{\tau}^{(1)} = (1+i\pi+2\ln s+4\gamma)\,\hat{\sigma}^{(0)} \tag{A 4}$$

$$\hat{\sigma}^{(0)} = -s\tilde{f}. \tag{A 5}$$

A.2. *Shear-stress layer*

The order-one vertical coordinate in the shear stress layer is $\zeta = Z^*/l = Z/\epsilon$.

$$\left.\begin{aligned} u_{\mathrm{d}} &\sim -\frac{\hat{\sigma}^{(0)}}{U(l)}\left[1+\frac{\epsilon}{\kappa U(l)}\{1-\ln\zeta-4K_0[2(\mathrm{i}s\zeta)^{\frac{1}{2}}]\}+O(\epsilon^2)\right],\\ w_{\mathrm{d}} &\sim -\frac{\hat{\sigma}^{(0)}}{U(l)}\left[-2\mathrm{i}s\frac{\epsilon}{\kappa U(l)}\kappa^2\zeta+O(\epsilon^2)\right],\\ \tau_{\mathrm{d}} &\sim -\frac{2\hat{\sigma}^{(0)}}{U^2(l)}\left[-1-4\zeta\frac{\partial K_0}{\partial\zeta}+O(\epsilon)\right], \quad p_{\mathrm{d}} \sim [\hat{\sigma}^{(0)}+O(\epsilon^2)]. \end{aligned}\right\} \tag{A 6}$$

A.3. *Middle layer*

The vertical coordinate is scaled on h_{m} so that $\hat{z} = Z/h_{\mathrm{m}}$. Furthermore, for a logarithmic approach flow, $\hat{z} = Z/\epsilon^{\frac{1}{2}}$ and $h_{\mathrm{m}}/L = \epsilon^{\frac{1}{2}}$.

$$\left.\begin{aligned} u_{\mathrm{d}} &\sim -\left[\frac{L}{h_{\mathrm{m}}}\tilde{f}U'+\frac{\hat{\sigma}^{(0)}}{U}\left\{1+UU'\int^{\hat{z}}\frac{\mathrm{d}z'}{U^2(h_{\mathrm{m}}z')}\right\}+O\left(\frac{h_{\mathrm{m}}}{L}\right)\right]\\ w_{\mathrm{d}} &\sim \mathrm{i}s\left[\tilde{f}U+\frac{h_{\mathrm{m}}}{L}\hat{\sigma}^{(0)}U\int^{\hat{z}}\frac{\mathrm{d}z'}{U^2(h_{\mathrm{m}}z')}+O\left(\frac{h_{\mathrm{m}}^2}{L^2}\right)\right], \quad p_{\mathrm{d}} \sim [\hat{\sigma}^{(0)}+O(h_{\mathrm{m}}/L)]. \end{aligned}\right\} \tag{A 7}$$

A.4. *Upper layer*

The vertical coordinate is scaled on L, so that $Z = O(1)$. By construction, the leading-order vertical velocity perturbation in the upper layer is determined by the transformation to the displaced coordinates.

$$u_{\mathrm{d}} \sim [s\tilde{f}\mathrm{e}^{-sz/L}+O(h_{\mathrm{m}}/L)], \quad w_{\mathrm{d}} \sim O(h_{\mathrm{m}}/L), \quad p_{\mathrm{d}} \sim -u_{\mathrm{d}}. \tag{A 8}$$

REFERENCES

ABRAMOWITZ, M. & STEGUN, I. R. 1972 *A Handbook of Mathematical Functions*. Dover.

BELCHER, S. E. 1990 Turbulent boundary layer flow over undulating surfaces. PhD thesis, University of Cambridge.

BELCHER, S. E. & HUNT, J. C. R. 1993*a* Turbulent shear flow over slowly moving waves. *J. Fluid Mech.* **251** (to appear).

BELCHER, S. E. & HUNT, J. C. R. 1993*b* A wall function for rapidly perturbed turbulent boundary layer flows. In preparation.

BRADLEY, E. F. 1980 An experimental study of the profiles of wind speed, shearing stress and turbulent intensities at the crest of a large hill. *Q. J. R. Met. Soc.* **106**, 101–124.

BRADSHAW, P. 1967 'Inactive' motion and pressure fluctuations in a turbulent boundary layer. *J. Fluid Mech.* **30**, 241–258.

BRADSHAW, P., FERRIS, D. H. & ATWELL, N. P. 1967 Calculation of boundary layer development using the turbulent kinetic energy equation. *J. Fluid Mech.* **28**, 593–616.

BRITTER, R. E., HUNT, J. C. R. & RICHARDS, K. J. 1981 Air flow over a 2-d hill: studies of velocity speed-up, roughness effects and turbulence. *Q. J. R. Met. Soc.* **107**, 91–110.

HUNT, J. C. R. 1973 A theory of turbulent flow round two-dimensional bluff bodies. *J. Fluid Mech.* **61**, 625–706.

HUNT, J. C. R. 1978 A review of the theory of rapidly distorted turbulent flows and its applications. *Fluid Dyn. Trans.* **9**, 121–152.

HUNT, J. C. R. 1984 Turbulence structure in thermal convection and shear-free boundary layers. *J. Fluid Mech.* **138**, 161–184.

HUNT, J. C. R., LEIBOVICH, S. & RICHARDS, K. J. 1988 Turbulent shear flows over low hills. *Q. J. R. Met. Soc.* **114**, 1435–1471 (referred to herein as HLR).

HUNT, J. C. R., NEWLEY, T. M. J. & WENG, W. S. 1990 Analysis and computation of turbulent boundary layers in varying pressure gradients. In *Proc. IMA Conf. on Computational Methods in Aeronautical Fluid Mechanics* (ed. P. Stow). Clarendon.

HUNT, J. C. R., TAMPIERI, F., WENG, W. S. & CARRUTHERS, D. J. 1991 Air flow and turbulence over complex terrain: a colloquium and computational workshop. *J. Fluid Mech.* **227**, 667–689.

JACOBS, S. J. 1987 An asymptotic theory for the turbulent flow over a progressive wave. *J. Fluid Mech.* **174**, 69–80.

JEFFREYS, H. 1925 On the formation of water waves by wind. *Proc. R. Soc. Lond.* A **107**, 189–206.

LAUNDER, B. E., REECE, G. T. & RODI, W. 1975 The development of a Reynolds stress turbulent closure. *J. Fluid Mech.* **68**, 537–566 (referred to herein as LRR).

MASON, P. J. 1986*a* On the parameterisation of orographic drag. In *Proc. ECMWF Workshop on Observation, Theory and Modelling of Orographic Effects*. ECMWF, Shinfield Park, Reading.

MASON, P. J. 1986*b* Flow over the summit of an isolated hill. *Boundary Layer Met.* **37**, 385–405.

MASON, P. J. & KING, J. C. 1985 Measurements and predictions of flow and turbulence over an isolated hill of low slope. *Q. J. R. Met. Soc.* **111**, 617–640.

MAXEY, M. R. 1982 Distortion of turbulence in flows with parallel streamlines. *J. Fluid Mech.* **124**, 261–282.

NEWLEY, T. M. J. 1986 Turbulent air flow over low hills. PhD thesis, University of Cambridge.

SMITH, F. T., BRIGHTON, P. M. W., JACKSON, P. S. & HUNT, J. C. R. 1981 On boundary layer flow past two-dimensional bodies. *J. Fluid Mech.* **113**, 123–152.

STEWARTSON, K. 1974 Multi-structured boundary layers on flat plates and related bodies. *Adv. Appl. Maths* **14**, 145–239.

SYKES, R. I. 1980 An asymptotic theory of incompressible turbulent flow over a small hump. *J. Fluid Mech.* **101**, 647–670.

TAMPIERI, F. 1987 Separation features of boundary layer flow over valleys. *Boundary Layer Met.* **40**, 295–307.

TAYLOR, P. A. & GENT, P. R. 1974 A model of atmospheric boundary layer flow above an isolated hill: an example of flow over gentle topography. *Boundary Layer Met.* **7**, 349–362.

TAYLOR, P. A., MASON, P. J. & BRADLEY, E. F. 1987 Boundary layer flow over low hills. *Boundary-Layer Met.* **39**, 107–132.

TOWNSEND, A. A. 1961 Equilibrium layers and wall turbulence. *J. Fluid Mech.* **11**, 97–120.

TOWNSEND, A. A. 1972 Flow in a deep turbulent boundary layer over a surface distorted by water waves. *J. Fluid Mech.* **55**, 719–735.

TOWNSEND, A. A. 1976 *The Structure of Turbulent Shear Flow*. Cambridge University Press.

TOWNSEND, A. A. 1980 Sheared turbulence and additional distortion. *J. Fluid Mech.* **98**, 171–191.

WENG, W.-S., HUNT, J. C. R., CARRUTHERS, D. J., WARREN, A., WIGGS, G. F. S., LIVINGSTONE, I. & CASTRO, I. 1991 Air flow and sand transport over sand dunes. *Acta Mechanica* (*suppl*) **2**, 1–22.

ZEMAN, O. & JENSEN, N. O. 1987 Modification to turbulence characteristics in flow over hills. *Q. J. R. Met. Soc.* **113**, 55–80.

ZEMAN, O. & TENNEKES, J. L. 1975 A self-contained model for the pressure terms in the turbulent stress equations of the neutral atmospheric boundary layer. *J. Atmos. Sci.* **32**, 1808–1813.

ZILKER, D. P. & HANRATTY, T. J. 1979 Influence of the amplitude of a solid wavy boundary on a turbulent flow. Part 2. Separated flows. *J. Fluid Mech.* **90**, 257–271.